Tailoring SOFC electrode microstructures for improved performance

P.A. Connor[a*], X. Yue[a], C.D. Savaniu[a], R. Price[a], G. Triantafyllou[a], M. Cassidy[a], G. Kerherve[b], D.J. Payne[b], R. C. Maher[c], L. F. Cohen[c], R.I. Tomov[d], B.A. Glowacki[d,e], R.V. Kumar[d], J.T.S. Irvine[a*]

a. University of St Andrews, School of Chemistry St Andrews KY16 9ST, Fife, UK

b. Department of Materials, Imperial College London, London, SW7 2AZ, United Kingdom

c. The Blackett Laboratory, Imperial College London, Prince Consort Road, London, SW7 2BZ, United Kingdom

d. Department of Materials Science and Metallurgy, University of Cambridge, 27 Charles Babbage Road, Cambridge, CB3 0FS, UK

e. Institute of Power Engineering ul. Mory 8, 01-330 Warsaw, Poland

Abstract

The key technical challenges that fuel cell developers need to address are performance, durability and cost. All three need to be achieved in parallel; however, there is often competitive tensions meaning that e.g. performance is achieved at the expense of durability. Stability and resistance to degradation under prolonged operation are key parameters There is considerable interest in developing new cathodes better able to function at lower temperature to facilitate low cost manufacture. For anodes, the ability of the SOFC to better utilise commonly available fuels at high efficiency avoiding coking, resistance to sulfur in bio-derived fuels and oxidation resistance at high utilisation are all key parameters. Optimising a new electrode material requires considerable processing development. The use of solution techniques to impregnate an already optimised electrode skeleton, offers a fast and efficient way to evaluate new electrode materials. It can also offer low cost routes to manufacture novel structures and to fine tune already known structures. Here we discuss infiltration and impregnation methodologies, look at spectral and surface characterisation and review the extensive recent efforts to optimise both cathode and anode functionalities. Finally we review recent exemplifications and look to future challenges and opportunities for the impregnation approach in SOFCs.

1. Introduction

The optimisation of solid oxide fuel cell (SOFC) electrode microstructures for improved performance has been a continual goal in the development of these devices. The critical areas of any fuel cell electrode microstructure are the triple phase boundaries (TPB). This is where electrons, ions and reactants meet and electrochemical reactions occur. Whilst this zone is extended with mixed ion conductors, the three phase boundary zone is still the focus of electrochemical activity. Thus, for good electrochemical performance, the TPB must have sufficient length and catalytic activity to allow electrochemical exchange to take place and move species across the boundaries. The stability of both the TPB and the catalysis to both time dependant ageing and changes in gas composition is vital in producing a robust, high performance and durable SOFC. These four features must be present in all good electrodes: porosity (gas “conduction”), ionic conduction, electronic conduction and sufficient catalytic activity. Some components may contribute to more than one feature. Additionally, the electrode must be stable under all the conditions it is likely to undergo in a fuel cell environment.

The anode is where the fuel oxidation takes place, and this has traditionally comprised of a porous cermet material containing nickel and yttria stabilised zirconia (YSZ). In this configuration the YSZ gives structural stability and also allows oxide ion conduction away from the electrolyte into the body of the anode. The nickel provides both the electrical conductivity and is also a catalytic surface

for the oxidation of the fuel (hydrogen gas in the simplest case). The porosity allows for the transport of the fuel into the electrochemical interfaces and triple phase boundaries. The close intermixing of these three phases gives an extended and diffuse interface over which the electrochemical reactions can take place and results in a very efficient electrode, which to date has proved very difficult to replace even though it has several significant technical issues such as degradation on redox cycling of the NiO to Ni and back,[1,2] carbon deposition from hydrocarbon based fuels[3] and sulphur poisoning.[4] There are of course engineering based solutions around these problems such as use of safe gases to prevent reoxidation in case of fuel gas loss, having steam in the system to promote reforming rather than cracking reactions, anode modification to reduce the propensity to coking/poisoning or the presence of a desulphurisation system upstream of the anode. However, most desirable is a fuel cell design that is tolerant to these problems making the whole system more robust.

The cathode is where the oxygen reduction reactions occur. A commonly used cathode composition is a composite mixture of YSZ and strontium doped lanthanum manganite perovskite ($La_{1-x}Sr_xMnO_3$) (LSM). Here the LSM provides the electronic conduction and catalytic functions and the YSZ the structural component and ionic conduction, with the porosity forming the triple phase boundary. [5] To further improve performance more recent cathodes have utilised mixed conductors such as strontium doped lanthanum cobaltite ($La_{1-x}Sr_xCoO_3$) (LSC) or strontium doped lanthanum cobalt ferrite ($La_{1-x}Sr_xCo_{1-y}Fe_yO_3$) (LSCF), where the mixed conduction nature of the material has greatly increased electrochemical exchange [6,7], not least by expanding the TPB by increasing the ionic conduction further over the surface. However, this increased performance comes at a cost because these materials systems have some issues with increased coefficient of thermal expansion, thermal stability and higher reactivity, with the most widely used doped zirconia electrolytes (especially during processing) leading to degradation and detrimental interfacial phase formation. [8,9] Although modifications to both composition and process protocols have reduced the impacts, it does constrain the system and reduces the options for optimisation.

The drive to lower operating temperatures for fuel cells to lower the materials cost of manufacture puts higher demands on the catalytic materials, requiring newer, more active materials, which often do not have the chemical and thermal stability as the bulk materials used for the electronic and ionic conductivity. This makes them difficult to add to a bulk process for cell fabrication. By separating the processing of the bulk, stable ceramic components from that of the catalytic components it becomes possible to tailor the processing of each and to optimise them for their specific requirements.

A particularly useful method for achieving this is impregnation, also known as infiltration, where a porous, skeletal ceramic support (a scaffold) is created which is then infiltrated with a liquid phase containing the desired component. The scaffold can be processed using traditional bulk ceramic methods to optimise porosity and mechanical attributes whereas the infiltrate can be dried and fired under a different, less harsh set of conditions, to result in tailored microstructures. This has the advantage of only placing the small amounts catalyst on the surface, where it can be active and not in the bulk where it is of less use. Because of this, impregnated electrodes often show higher power density and lower resistance compared to electrodes fabricated using traditional techniques. [10, 11,12] Clearly impregnation of electrodes is a low cost route to fabrication and, if applied successfully to give suitable nanostructured interfaces, enhanced performance will be delivered. Thus the real underlying challenges are to combine performance with durability and then to advance the technique to large scale manufacture.

The terms impregnation and infiltration will be used interchangeably throughout this work, as they are in the literature.

1.1 Methodologies

There are three basic methods for impregnation:

(A) Impregnation with metal-salt solutions with various additives (urea, citric acid, glycine, ethylene glycol, etc.).
(B) Impregnation with nanoparticles in suspension.
(C) Molten salt impregnation.

The use of metal salts (A) is the simplest and most common method also having the greatest flexibility in the choice of solvent and additives. In most cases, metal nitrates are used, dissolved in water or alcohols. The use of a surfactant is beneficial for facilitating the penetration of solution inside the porous structure by reducing the surface tension. It does however require multiple infiltration cycles in order to achieve high loading levels and there can be a non-uniform distribution of the infiltrate depending on how the initial solution and the resultant compound wet the surface. The use of nanoparticles (B) allows the synthesis of the catalyst phase in advance, but the inks are difficult to stabilise and may clog the pores leading to gas diffusion obstruction. The use of molten salts (C) facilitates uniform high loaded infiltration but is more complicated and so less common in electrochemical applications.

The choice of material for the porous ceramic framework depends on the desired properties and the design of the cell. The scaffold must perform at least two of the basic features of the electrode. It must be porous, and ideally chemically/structurally stable under all operating conditions. It will also be either electronically conducting or ionically conducting, with the other phase produced by impregnation, or ideally both an ionic and electronic conductor (mixed ion/electronic conductor, MIEC), with an impregnated catalyst. Often to get the desired performance multiple species both catalytic and conductive may be impregnated. This choice of scaffold and impregnate gives rise to several generic microstructures. These are: dispersed catalyst on an electron conducting scaffold, and ionic conducting scaffold with connected mixed or electron conducting catalyst or percolating electron catalyst on an ionic conducting scaffold.[13] These are shown schematically in Figure 1.

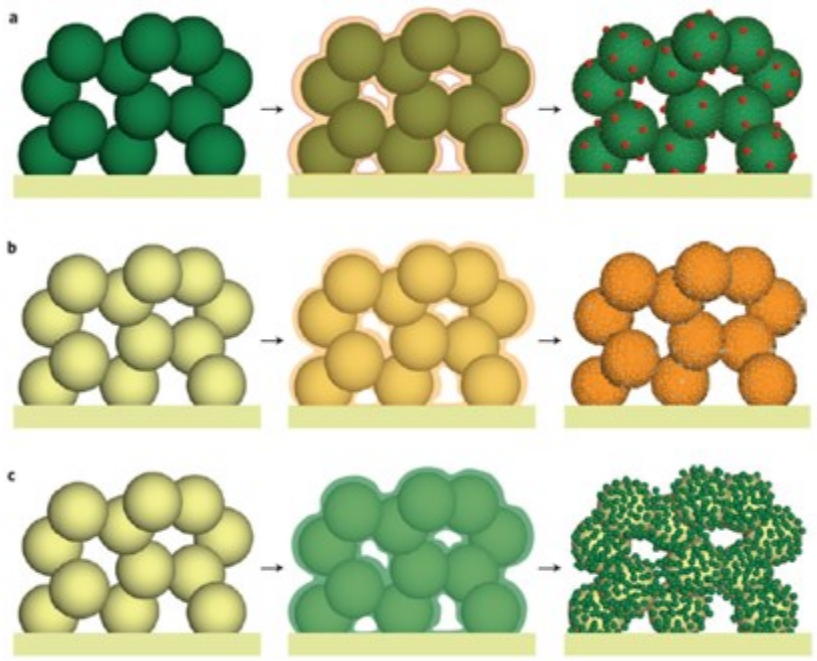

Figure 1 Examples of microstructures evolved from impregnation a) An electron conducting backbone (green) is infiltrated with precursor (orange) which forms dispersed catalyst particles across the surface. This can be a single material or multiple phases. b) An Ionic conducting backbone (yellow) is coated with precursors, which will form a continuous electron or mixed ion electron conducting perovskite phase (orange). In some cases surface morphology may change with atmosphere to increase triple phase boundary. c) An Ionic conducting backbone (yellow) is coated with precursors, which will form a percolating network of electronic conducting particles. [Modified from Ref.13]

This brings up a number of interesting questions with respect to wetting, the interaction of surfaces and surface energies at various points in the infiltration process. Firstly, one would expect the surface energy of the precursor solution to be instrumental in both how the solution penetrates the porous scaffold and also how it then deposits onto this surface. This will of course vary with each set of solution and scaffold materials. Secondly, even after the heat treatment to form the initial catalyst phase the wetting and interaction of the scaffold and catalyst surfaces continue to play a central role in the stability and durability of the electrode. Therefore, a deeper understanding of how the various phases present in an electrode interact is vital to improve design and optimisation of these systems.

The interactions of the impregnated catalyst particles with the scaffold surface and the gas species controls the catalytic behaviour observed. With the presence of nano-sized particles this may not have the same behaviour as given by the bulk materials and so observations of the electrodes while operating is also needed, to optimise the amount and type of impregnated species. This needs observation at long distance by spectroscopic techniques such as XPS or Raman, which can observe the evolution of electrodes under realistic conditions of elevated temperature, and air or reducing gases.

An early example of work on infiltration was focussed on overcoming the limitations of nickel coking in hydrocarbon fuels. One potential catalyst of interest was copper, which showed very low propensity to promote coking. However the low melting point of both copper and copper oxide, which was below the temperatures required for the bulk ceramic processing routes prevented the use of a bulk Cu/YSZ cermet. By infiltrating a porous YSZ scaffold with a copper nitrate solution then decomposing this to the oxide, it was possible to produce a finely dispersed copper catalyst at temperatures well below the melting points of both the oxide and metal which offered the opportunity for a high performance anode with good carbon tolerance. [14] However even though the melting point issues could be avoided during processing, the metallic copper still proved too mobile at operational temperatures, leading to large scale agglomeration and so rapid deactivation of the anode. [15]

This review will briefly touch on the wetting and observation of the impregnated electrodes before discussing various anode and cathode systems.

1.2 Wetting and impregnation

The interactions between a liquid and a solid or indeed a solid with another solid is determined by the surface energy of the materials and the interfacial energies of the systems so formed. This is usually expressed as a wetting process, with thin even coatings coming from positive surface interactions (good wetting) or small dispersed particles from poorly wetting systems. The traditional measurement to investigate the interfacial properties of a system is the sessile drop technique, where the contact angle of the edge of a drop of a liquid lying on the surface of a solid substrate is measured in thermodynamic equilibrium. By measuring the contact angle of various liquid-solid

interactions the surface energies of the solid can be obtained. [16,17,18,19,20] Wetting behaviour of various liquid-solid ceramic interactions have been studied in, for example, sodium batteries[21], direct carbon fuel cells[22], and the use of ceramic-glass seals for SOFCs. [23,24,25,26] There is, however, little work on the wetting properties for impregnation of SOFCs.

During the impregnation there are two sets of surface interactions, the first one being the solution in contact with the dense walls of the porous scaffold creating a solid-liquid interface. The ability for the solution to move through the porous substrate is highly dependent on the interfacial energy of the system, which again depends on the specific surface properties of the solution and the solid. [25] The other surface interaction is the solid-solid surface interactions during the thermal treatment for sintering the final impregnated materials where the surface energies control the size and shape of the final catalyst. Therefore to understand the processes forming the impregnated catalyst materials the surface properties of the support, the solution and the final material need to be known.

The reported studies on impregnation cover the wetting of the impregnate solution on the various substrates and how it penetrated into the porous scaffold. This was typically done by simple measurement of the contact angle of the impregnate solution on a polished dense surface of the scaffold material. This allows the tuning of the solvent (and additives)[27] resulting in reasonable infiltration. A number of surfactants have been used including Triton-X100 and X-45[28, 29, 30, 31], 2-butoxyethanol [32], CTAB[33] or Pluronic P123 (BASF Corp)[34]. Several studies by Lou et al. [28,35, 36, 37] have shown that tuning the wetting properties of the infiltrate ink with organic solvents was another efficient way to improve the wettability on scaffold grains.

This however does not cover the solid-solid interaction of the final formation of the catalyst. This is very difficult to measure directly, and so the surface energy of the materials is measured separately leading to the calculation of the surface energy, and hence type of interaction. The methodology to study the interactions has been led by MetLab at the University of Patras. The extraction of the surface energy usually requires the application of a combination of experimental methods multiphase equilibration technique[16,17,18,19,20,38] or indentation technique [39]. For this reason, most of the literature data have been derived from theoretical evaluations[40]. The underlying physical processes are well understood and can be described by a set of empirical and semi-empirical equations. [41,42] The surface energies of the liquid metals are known,[43] as are the polar and the dispersion forces contribution, the surface energy of all the polar liquids used [44,45,46] which can be used to get the surface energies of Alumina[18 43], zirconia[19], Y_2O_3 [47], YSZ[20] and Ceria[38], over a range of temperatures.

The power of these surface measurement can be observed in the mixed ionic electronic conductor yttrium and titanium doped zirconias/Ni metal system[48,49] where the Ti content of the ceramic changed both the measured contact angle, and hence surface energy, and the electrode performance. This allowed the ceramic to be optimised for the best interaction with the Ni phase.

These fundamental measurements are required in order to understand the processes happening during impregnation, ultimately leading to practical control or design of materials. However, this work is still under-valued and needs significantly more research to establish a robust framework.

2. Observation of infiltrated electrodes

Once made, the impregnated electrodes need to undergo electrochemical testing and observation, in order to correlate electrochemical performance with microstructure. The development of high-resolution microscopy has been very helpful to study the nano-structured SOFC electrode and to

develop an understanding of the microstructure-performance relationship.[50] The use of in-situ or at least in operando techniques such as Raman or XPS provides useful mechanistic information.

The various microscopy and spectroscopic methods that have been used to study conventional SOFC electrodes in situ or in operando are covered elsewhere.[51] To obtain chemical information about SOFC electrodes in operando, spectroscopic methods are needed to collect data from a distance due to the high temperature and need for gas environment. This limits methods to those based on photons such as: Emission IR[52], Raman[53], X-ray Diffraction (XRD)[54], (Ambient pressure) X-ray Photoelectron Spectroscopy ((AP)XPS)[55,56], and the various x-ray absorption (XAS) methods (XANES, EXAFS etc)[55,57].

To study impregnated electrodes, the techniques also need to be both surface sensitive and give chemical information about the catalytically active surface species. IR gives information about the species adsorbed to the surface and not the surface itself, but is difficult perform at hot IR emitting electrodes. XRD principally gives information about the bulk of the majority phase, and so is less sensitive to the smaller volume impregnated phases. The various x-ray absorption methods need a high intensity source such as a synchrotron and so are less available and thus have not been greatly applied to infiltrated electrodes as yet. An exception to this is a recent study on infiltrated LSCF sintered porous powder cathodes using synchrotron ultra-small angle x-ray scattering (USAXS). This allowed the evolution and growth of nanoparticles of LSC and lanthanum zirconate particles to be followed through liquid phase impregnation and subsequent annealing.[58] Clearly such X-ray absorption methods are an important approach that will be widely applied in the future.

Probably the most available and informative methods are Raman and XPS. Raman is surface sensitive and gives observations on the metal oxide vibrations of both the scaffold and impregnate phase. It is also based on visible light, and so has less problems with the IR emission of the hot electrodes. XPS, or for in operando work Ambient Pressure XPS, gives both the elements present on the surface and their oxidation states, and how they change under fuel cell conditions. These two techniques are the ones most used for impregnated electrodes.

2.1 In-situ Raman

Raman spectroscopy[59] is a chemically specific, non-invasive, optical characterisation technique usually used in combination with a scanning modality that provides diffraction limited spatial information and mapping. It has been widely employed to provide insight regarding the processes that occur in SOFC materials during or after operation[60]. Raman is best described as a near-surface characterisation technique because the optical penetration depth typically ranges between 10s of nanometers to a micron depending on the porosity, material composition, the oxidation state of the materials under study and the laser wavelength used. The combination of near surface sensitivity, chemical specificity and high spatial resolution means the technique is well suited to examining the impact of impregnation on the reaction kinetics within a SOFC environment.

Raman spectroscopic investigations of SOFCs can be broadly grouped into three subsets – *ex-situ*, *in-situ* and *in-operando* with *ex-situ* characterisation being the easiest to perform and *in-operando*, requiring specialised bespoke equipment[61], the most difficult. Although not yet widely studied, Raman spectroscopy can provide key information regarding the effectiveness of impregnation via any of these types of measurement. Over the last decade, *in-situ* and *in-operando* Raman spectroscopy has been developed to investigate reaction kinetics[62], reaction intermediates, temperature distributions[63], sulphur poisoning[64,65,66], material oxidation states[67] and SOFC operation on carbon fuels[68] under realistic operating conditions. Raman has been particularly successful in studying processes that are critically dependent on the characteristics of the TPB such as carbon

deposition and redox interactions across the TPB[69]. Figure **2** shows an example of how Raman can be used to investigate redox interactions in SOFC materials at the TPB. Figure **2** A shows a typical Raman spectrum obtained *in-situ* from a gadolinium doped ceria (cerium gadolinium oxide, CGO)-NiO cermet using a 514nm laser. The main peak at approximately 450cm^{-1} is the F_{2G} mode of Ceria while the broader peak at approximately 1100 cm^{-1} is a combination of NiO overlapping with a second order mode of the CGO. Both of these peaks are directly related to the oxidation states of the two materials and can be used to monitor their relative oxidation states in real time. Figure 2B shows the integrated intensity of the Ceria peak for both pure and composite CGO as a function of time while the sample is exposed to dry hydrogen. The CGO in the cermet is observed to reduce more quickly and to a greater extent than the pure CGO due to the hydrogen spillover across the TPB from Ni to CGO. This process is shown schematically in Figure **2** C. Finally the effect of the Ni is seen more clearly on the reduction of the same materials during reduction in humidified hydrogen as shown in Figure **2** D. These results are discussed in more detail in Maher et al,[69] but clearly show how Raman could be used to study the effects of impregnation of SOFC anodes on their redox properties.

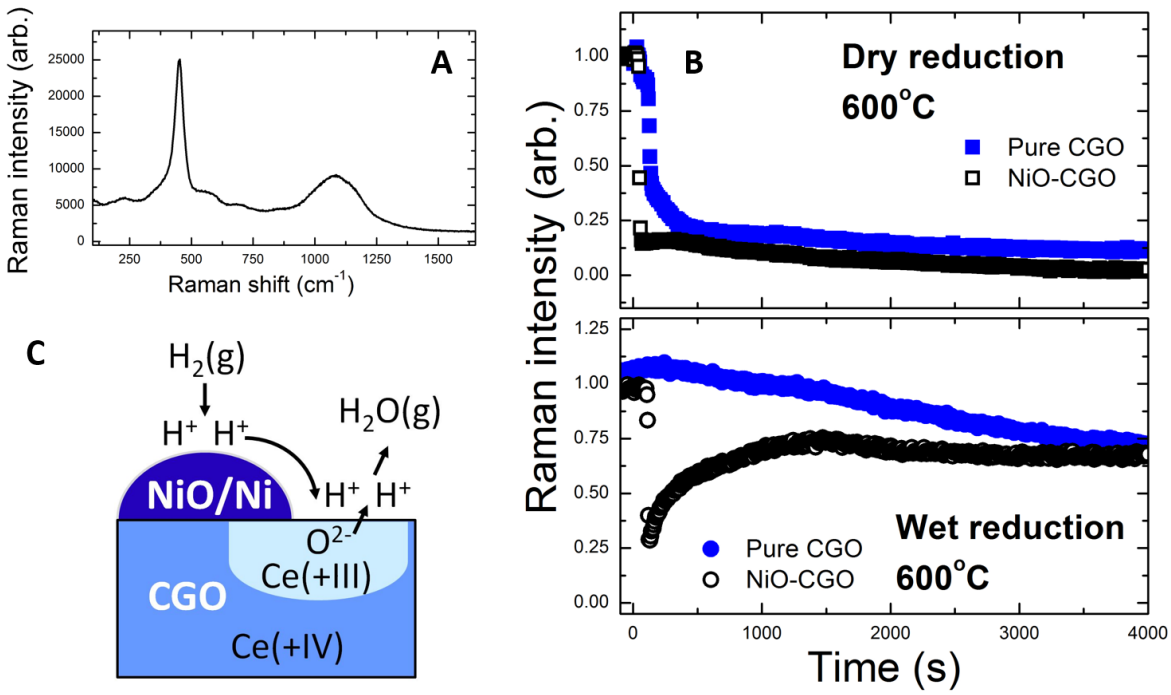

Figure 2 A: An example Raman spectrum of CGO-NiO cermet *in-situ* at 600°C. B: Example *in-situ* Raman monitoring of the reduction of CGO-NiO cermet and pure CGO in dry and wet (humidified to 3% H_2O) hydrogen. CGO reduces faster and to a greater extent when combined with NiO. This is due to the spillover of hydrogen from the Ni to the CGO at the TPB and the effect of the hydrogen spillover over the TPB is even larger in the wet gas.. C: Schematic illustration of the hydrogen spillover process. . Adapted from Advanced Science, **2016** 3 (1), 1500146 [63] (CC BY 4.0)

Raman has been found to provide particularly rich information regarding carbon deposition on SOFC anodes, in particular Raman peak ratios reveal details of the crystallinity (graphitic vs amorphous), and the relative amount of carbon present as well as their location [63,70]. Understanding the specifics of the carbon deposition mechanism on SOFC anodes is key to developing strategies to improve their resistance, which would allow for a greater flexibility in the choice of fuel. A wide range of fuels including methane, methanol and higher alkanes as well as complex fuel mixtures approximating biogas [71,72,73,74,75,76] have been investigated while the effect of anode modifications such as specific

composition and catalyst enhancement (adding small amounts of precious metals for example) has also been characterised extensively [77,78,79]. Patterned electrodes combined with high resolution *in-situ* mapping has allowed TPBs to be precisely controlled and carbon deposition characterised as a function of distance from it[80]. Such measurements help to improve our understanding of how changes in the TPB affect carbon deposition and could be extended to study other critical processes. As a result, they are directly relevant to understanding the effects of impregnation of anodes given the close control of the TPB impregnation techniques allow.

2.2 X-ray photoelectron spectroscopy (XPS)

X-ray photoelectron spectroscopy (XPS) is (principally) an ultra-high vacuum (UHV) surface characterisation technique used in the investigation of the chemistry and physics of materials[81]. It provides quantitative information about the elemental composition and chemical environment (e.g. oxidation state) of the surface and can be a useful technique to examine the active redox couples, such as the oxygen storage/release property of the ceria-based solid solution and the chemical states of the dopant and the host ions. The reversible CeO_2 – Ce_2O_3 reduction transition associated with oxygen-vacancy formation and migration is directly coupled with the process of localization/delocalization of the 4*f* electron of cerium[82]. Traditionally, a significant drawback of the technique is the inability to study samples in anything other than under UHV conditions (i.e. 10^{-9} mbar or lower). As a result, most of the studies found in the literature on solid oxide fuel cell were investigated using standard XPS. An important point to note is that the principal core level of cerium, the 3*d*, has a very complex line shape. An example of a fitted spectrum of the Ce 3d core level is shown in Figure 3 for CeO_2 infiltrated on porous YSZ. The complexity of the Ce *3d*, has been fully described by Kotani et al.[83], where it originates from the close proximity of the 4*f* level of the CeO_2 to the O 2*p* valence band with which it hybridises. This requires careful peak fitting of the resulting spectra, and depending on the composition can require up to 10 peaks being required for an accurate and representative fit. For stoichiometric CeO_2, the Ce^{4+} chemical environment gives rise to six peaks, observed at the (on average) binding energy positions of 882 eV (v), 888.7 eV (v''), 898.2 eV (v'''), 900.7 eV (u), 907.3 eV (u'') and 916.4 eV (u'''). The designations (u',v'…etc) denote the range of final states available from the photoemission process. Non-stoichiometric CeO_{2-x}, with the Ce^{3+} present in the material, gives rise to a further four peaks, found at (average) binding energy position of 880.4 eV (v_0), 884.2 eV (v'), 898.3 eV (u_0) and 902.5 eV (u'). In total there are up to ten peaks in a single Ce 3d spectrum, not including any other core levels from other elements that could be present due to overlapping binding energies. The following section gives a brief overview of previous XPS studies of ceria found in the literature.

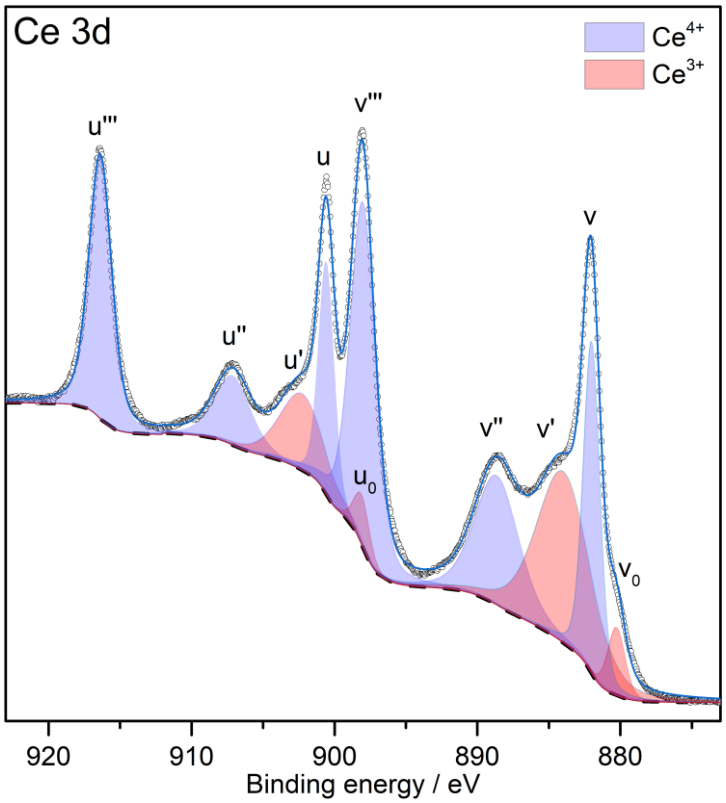

Figure 3. Ce 3*d* XPS spectra from the CeO_2 infiltrated on porous YSZ (dots), fit (solid blue line), Shirley-type background (dashed line), and components assign to Ce^{4+} (light blue) and Ce^{3+} (light red).

Henderson et al.[84] used XPS, as well as temperature programmed desorption (TPD), to investigate the surface chemistry of water on the oxidized and reduced surfaces of a thin film of CeO_2 (111) on YSZ (111). They quantified the level of reduction using the Ce3$d_{3/2}$4f_0 photoemission peak at 917 eV (u''') resulting from Ce^{4+} sites. By comparing with literature studies of reduction of single crystal CeO_2 (111), they found that the volume-to-surface ratio of ceria samples influences partly the reduction conditions, and finding detectable levels of surface Ce^{3+} sites. Hegde et al.[85] undertook a structural investigation using XPS, XRD and H_2-TPR, of transition metal, noble metal, and rare-earth (R.E.) ion substituted ceria and found a relationship between the oxygen storage capacity (OSC) and structural changes induced by the dopant ion in CeO_2. They found that transition and noble metal ion substitution in ceria greatly enhances the reducibility of $Ce_{1-x}M_xO_{2-\delta}$ (M= Mn, Fe, Co, Ni, Cu, Pd, Pt, Ru), whereas R.E. ion substituted $Ce_{1-x}A_xO_{2-\delta}$ (A = La, Y) has little effect in improving the OSC. Jiang et al. [86] investigated infiltrated Pd nanoparticles catalyst on Ni/GDC as these particles are the most widely studied catalysts for the O_2 reduction and in particular the hydrocarbon oxidation reactions. Using XPS they found the existence of the Pd/PdO_x redox couple during the H_2 oxidation reaction which are most likely the cause for the enhanced adsorption and diffusion processes of the H_2 oxidation reaction on the surface of the Ni/GDC anode.

Recently, there has been significant improvement of the electrostatic lens system of the hemispherical analyser using in photoelectron spectroscopy, allowing surfaces to be investigated by XPS whilst at pressures of several mbar of a gas. With a growing number of investigations using ambient pressure X-ray photoelectron spectroscopy (APXPS) of operando SOFCs being carried out using this technique [87,88,89,90,91,92]. Zhang et al.[87] was the first (APXPS) study of an operating solid oxide electrochemical cell. The device consisted of a CeO_{2-x}/YSZ/Pt single-chamber cell and was studied under 1 mbar of H_2 and H_2O gases at a temperature of 750 ˚C. The mixed ionic/electronic conducting CeO_{2-x} electrodes underwent Ce^{3+}/Ce^{4+} oxidation-reduction changes with applied bias.

APXPS measurements of local surface Ce oxidation states while applying electric potentials reveal the active ceria regions during H_2 electro-oxidation and H_2O electrolysis. This demonstrated that the active electrochemical region extends approximately 150 µm away from the current collector and that significant shifts from the equilibrium surface Ce^{3+}/Ce^{4+} concentrations were needed to drive the electro-oxidation of H_2 and the electrolysis of H_2O. Nenning et al.[90] also studied an operando SOFC, this time of a LSC ($La_{0.6}Sr_{0.4}CoO_3$) cathode and an STF ($SrTi_{0.7}Fe_{0.3}O_3$) anode under high temperature and pressure conditions. Their study revealed that in an oxidizing atmosphere all materials exhibit additional surface species of strontium and oxygen, and that cathodic polarization in reducing atmosphere leads to the reversible formation of a catalytically active Fe^0 phase.

Gabaly et al.[89] studied the different oxidation steps of a Ni electrode from Ni/YSZ/Pt SOFC using operando APXPS. They found that there are three distinct steps in the oxidation of the Ni anode in a hydrogen environment. In the first two steps, the Ni exposed to the gas remains metallic, but the Ni at the interface between the anode and the electrolyte YSZ is oxidized. In a third step, they claim that the Ni oxidises in the form of NiOOH, a species not previously reported in the literature of these SOFC materials.

3. Impregnated Anodes

There are a number of review papers available on infiltration of SOFC anodes, focused in large part on metal based cermet anodes and on some ceramic based anodes, including (La, Sr)(Cr, Mn)O_3 (LSCM) and $SrTiO_3$.[10,93,94,95] Here we will review the very recent progress in the development of impregnated SOFC anodes (or fuel electrodes in SOECs) since the last review paper in 2013, following the types of scaffold used. Some previous work will be included from a different perspective.

3.1 Electrolyte material based porous scaffold

Impregnation into YSZ based frameworks has been most widely studied, as it ensures the mechanical stability, good contact and matched thermal expansion between electrode and YSZ electrolyte. Many materials have been applied to a YSZ based anode via impregnation including M (Ni, Cu, Co)/ceria,[10,96,97,98,99] LSCM,[100,101,102,103] (La, Sr)(Sc, Mn)O_3[104] etc. See also the previous reviews on these materials. [10.93,94,95,] Of the various catalysts being introduced into YSZ scaffold, (La, Sr)(M,Mn)O_3 (M= Ti, Cr) stands out with unique morphology on the surface of YSZ.[100,102,103] Corre et al.[103] found that, after solution impregnation and high temperature sintering in air, the resulting LSCM forms a thin smooth film on top of YSZ grains, which resembles a liquid wetting on a solid surface and is in great contrast with most of the other impregnates that often appear as discrete or aggregated particles, patches, or flakes on the scaffold after sintering. As shown in Figure **4**, this smooth coating of LSCM breaks into interconnected nanoparticles upon reduction which offers extensive triple phase boundaries for the H_2/CH_4 oxidation reaction, as well as CO_2 reduction reaction. [102] The wetting of LSCM on YSZ is restored after switching back to oxidising atmosphere. It was proposed that this interesting phenomenon is related to the interactions between Mn and YSZ scaffold, thus the wetting only happens when Mn is present, with the degree of wetting varying with the Mn concentration in the perovskite. The wetting of LSCM on top of YSZ in air and its de-wetting in reducing conditions provide an ideal concept for designing high performance SOFC anode through impregnation.

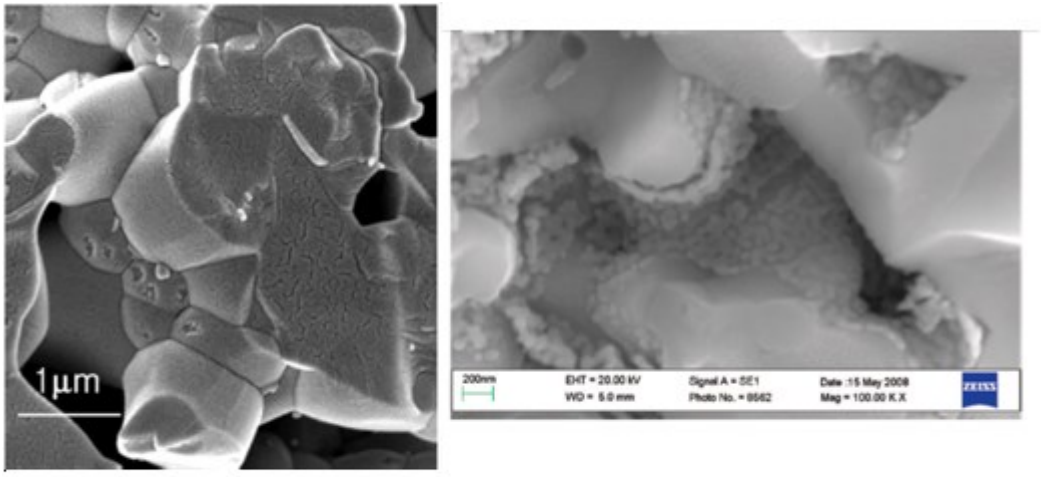

Figure 4 Infiltrated LSCM microstructures showing morphology change in differing atmospheres a) from fairly continuous in oxidising (calcination in air at 1200 ˚C) to b) distinct nanoscale grains in reducing atmosphere (5 hours in humidified H_2 (3% water). Reprinted with permission from *Chemistry of Materials* **2009**, *21*, 1077. Copyright 2009 ACS Publications**.**

Xia et al. [105] created a novel YSZ scaffold structure by phase-inversion tape casting method, and the resulting microstructure featured channelled pores with graded pore size and porosity in gas delivery layer and electrochemical reaction layer. The double perovskite $Sr_2Fe_{1.5}Mo_{0.5}O_{6-\delta}$ (SFM) was infiltrated into this graded porous YSZ scaffold, forming a highly continuous network giving electronic conduction on the surface of YSZ scaffold. Remarkable performance was demonstrated from this novel nanostructured SFM-YSZ fuel electrode in both fuel cell and electrolysis cell operations (without safe gas which is usually necessary for Ni-YSZ cermet electrodes). At 800 ˚C with H_2 (3% H_2O), a peak power density of 1.08 W cm^{-2} was achieved in fuel cell mode, higher than that from a Ni-YSZ electrode (0.8 W cm^{-2}) under the same conditions; the current density values reached 1.1 A cm^{-2} and 1.46 A cm^{-2} at 1.5V in electrolysis mode with dry CO_2 and CO_2-H_2O respectively. The infiltrated SFM-YSZ also exhibited good stability in a short-term test at 1.3V for CO_2-H_2O co-electrolysis, indicated chemical stability between SFM and YSZ at below 1000 ˚C.

The main issue with using a YSZ framework is that due to its purely ionic conductive nature it poses problems for efficient electronic processes such as charge transfer and current collection. There needs to be a large amount of highly electronic conducting phase added to overcome these problems, which in turn compromises the performance and durability of the impregnated anode due to the high tendency of nanoparticles to coarsen. Work continued with YSZ scaffold has been related to improving the thermal stability and poor electrochemical activity of Cu/Ceria based anodes.[106,107] Dual metal infiltration has been found to be advantageous for retaining the uniform dispersion of metal-ceria network and mitigation of the aggregation of Cu particles, and thus optimised morphology and reinforced electrochemical performance. Basu et al. incorporated Fe into the Cu-CeO_2-YSZ anode matrix and used various techniques to investigate the structural, morphological and electrochemical properties of dual metals /CeO_2 based anode.[106] With the presence of Cu, the reduction of iron oxide was promoted; whilst at the same time, the presence of Fe improved the dispersion of Cu-ceria network, enabling a better electrical connectivity between Cu, Fe, and ceria catalyst particles, which reduced the sintering of Cu to some extent. These contributed to a higher maximum power output observed on the Cu-Fe-CeO_2-YSZ anode for H_2 and CH_4 oxidation at 800 ˚C. However, stability of such an anode (with 1wt% Pd to further enhance oxidation activity) was still a concern after a short-term operation (~46hrs) in CH_4 fuel at 800 ˚C at 0.6 V. Performance decreased from 125 to 100 mW cm^{-2} during 20-23 hrs, which was due to both the sintering of catalyst and

carbon deposition. Poor carbon tolerance was also reported on Pd (0.5wt%) and Pd/CeO_2 impregnated LSCM-YSZ composite anode for CH_4 oxidation, while in contrast, high resistance to coking was observed on Pt and Pt/CeO_2 containing anode among Ni, Pd, Pt and Ceria catalysts.[108]

The interplay between multiple infiltrated phases was found of great importance in maintaining the metal catalyst small size, compared to only metal impregnation. Boaro et al. investigated the effect of redox treatments on the morphology and performance of SOFC anodes prepared via infiltration of Cu and $Ce_{0.5}Zr_{0.5}O_2$ (CZ) into porous YSZ skeleton.[107] The infiltrated CZ showed higher reducibility and electronic conductivity under SOFC operating conditions above 800 ˚C, however, it was suggested that a structural change to a pyrochlore phase might happen in CZ, which would impose mechanical stress on the electrolyte/electrode interface and cause delamination. On the other hand, an in-situ redox cycle at 700 ˚C led to significant increases in the power density of a Cu-CZ/YSZ//YSZ//YSZ/LSM cell in 3% humidified H_2-air, which was due to the rearrangement of the morphology and microstructure of the CZ oxide at the electrode/electrolyte interface and to the redistribution of copper leading to improved Cu-CZ connectivity. This is clearly supported by the SEM shown in Figure 5. The interplay between Cu and CZ plays a fundamental role in determining the anode electrochemical activity.

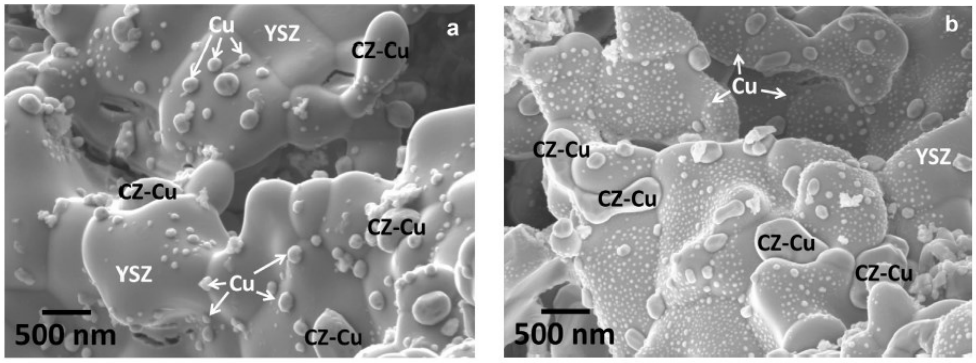

Figure 5 SEM images of a porous YSZ infiltrated with 10wt% Cu and 20 wt% CZ, before (a) and after oxidation at 700 ˚C and subsequent reduction (b). Reprinted with permission from *Journal of Power Sources* **2014**, *270*, 79. Copyright 2014 Elsevier**.**

Gadolinium doped Ceria ((Gd, Ce)O_2, GDC) electrolyte material has also been used as a porous skeleton with subsequent infiltration as SOFC anodes.[109],[110] Ni impregnation was conducted into a GDC scaffold that was produced with a mixture of nano-scale (5 nm) and larger commercial (0.5 μm) powders.[109] The addition of nano-sized particles allowed increased porosity and better sintering of the GDC scaffold at reduced temperature as low as 1000 ˚C. Han et al. investigated the impregnation of $Sr_2Fe_{1.5}Mo_{0.5}O_{6-\delta}$ (SFM) into a porous GDC skeleton based on SOFC with GDC as electrolyte. The ohmic resistance at 600 ˚C for a SFM-GDC electrode decreased from 0.82 Ω cm^2 for a traditional composite to 0.48 Ω cm^2 when prepared via impregnation. The polarization resistance from the impregnated anode was also significantly reduced. Furthermore, fairly good durability was observed on the impregnated anode fuelled by H_2 with 100ppm H_2S, indicating excellent sulfur tolerance from the SFM impregnated GDC anode.

Treating the scaffold surface prior to impregnation can be used to tailor the electrode microstructure and its electrode properties. De Guire et al. treated the NiO-GDC SOFC anode with some organic surfactants, including thiol (1-dodecanethiol, $CH_3C_{11}H_{22}SH$) and sulfonate, before depositing nanocrystalline ceria from aqueous solution, and studied the role of these organic surfactant pre-treatments on ceria microstructure and sulfur tolerance at various SOFC operating conditions.[111] The functional groups introduced from the surfactant pre-treatment impacted on the attachment of the subsequent GDC coatings to the substrate and their distribution on the substrate.

It was found in this study that a thicker and more uniform ceria coating was produced from the thiol pre-treatment than from the sulfonate pre-treatment. As a result, the direct or thiol treated ceria/Ni-GDC anode provided the best sulfur tolerance with the idea that ceria nanoparticles may act to impede the sulfur adsorption on Ni which degrades cell performance significantly.

3.2 Perovskite based scaffolds

The use of ceramic anodes based on perovskite materials has been proposed for improved robustness.[112] On reduction, in typical conditions present in the fuel electrode, these materials exhibit reasonable electronic conduction and excellent redox stability, contributing to a good electrode performance. The lack of catalytic activity towards fuel oxidation can be compensated by impregnation of catalytically active materials. In a method which is similar to that described above, appropriate mixtures of nitrate precursor solutions can be infiltrated in the perovskite framework that was pre-fired at high temperature. Both of the most common perovskite anodes, $(La_{1-x}Sr_x)(Mn_{0.5}Cr_{0.5})O_3$ (LSCM) and $(La_{1-x}Sr_x)TiO_3$ (LST), have been successfully infiltrated in this way.[9,12]

3.2.1 Perovskite LSCM based scaffold

The perovskite LSCM has been considered as alternative anode material to replace Ni-cermet because of its mixed electronic and ionic conductivity, electrochemical activity for the oxidation of a range of fuels, including methane, and superior resistance to coking and sulfur poisoning.[113,114] Nonetheless, the electrochemical properties of LSCM on its own are often not sufficient to facilitate the fast oxidation reactions needed at the anode, especially when it has been sintered at high temperature to make good contact with dense electrolyte. Its electronic conductivity is low in low p_{O2} atmospheres due to the p-type conductivity in LSCM. Therefore, it is essential to add both catalytically active and highly conducting phases to improve its anode performance.[115,116]

Metal impregnations on porous LSCM anodes have been tested in SOFC operated for H_2/CH_4 oxidation and in SOEC for steam-carbon dioxide co-electrolysis.[117,118] Different amount of Co on pure LSCM anode were prepared and tested.[117] The Co loading was vital to ensure good electronic conduction and sufficient catalytic activity, with small amounts leading to scattered Co particles on the surface of LSCM, thus poor electronic conduction, and a very high loading forming a core-shell structure that contains dense Co particles on the surface of the LSCM core (Figure 6). The core-shell structure was found detrimental for efficient gas transportation to the active sites in LSCM based anode. Cu-infiltrated porous LSCM was used as the fuel electrode for steam-CO_2 co-electrolysis cell, with LSGM electrolyte and LSCF oxygen electrode.[118] The introduction of Cu (20 wt%) improved the electronic conductivity of the electrode effectively, thus significantly lowered ohmic resistance was observed. Despite much improved performance due to metal impregnation, the absence of an oxide ion conductor in metal modified LSCM anode may restricts the reaction active sites to the electrode/electrolyte interface, originated from the fairly low ionic conductivity in LSCM in reducing atmosphere. To get around this problem, a LSCM/$Sm_{0.2}Ce_{0.8}O_2$ (SDC) composite backbone was used as the support for a vanadium pentoxide (V_2O_5) nanocatalyst for CO_2 electrolysis.[119]

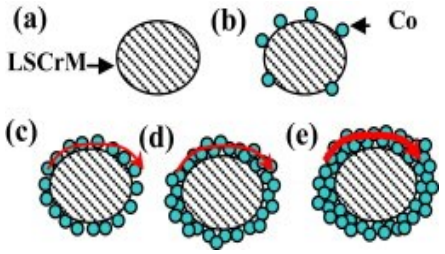

Figure 6 Model of LSCM backbone impregnated with: (a) 0 mg cm^{-2} Co, (b) 0.56 mg cm^{-2} Co, (c) 1.66 mg cm^{-2} Co, (d) 2.22 mg cm^{-2} Co, (e) 3.88 mg cm^{-2} Co. Reprinted with permission from International Journal of Hydrogen Energy **2014**, 39, 7980. Copyright 2014 Elsevier.

The impregnation of mixed electronic and ionic conducting material, such as doped ceria, is advantageous, offering both higher conductivity and good catalytic properties compared with a metal impregnation. The effect of $Sm_{0.2}Ce_{0.8}O_2$ (SDC) impregnation on the electrochemical performance of LSCM anode was investigated by Zhu et al in SOFC running with 5-10% H_2/Ar.[120] With the aid of electrical conductive relaxation (ECR) measurements, it was observed that the surface exchange coefficient was improved by a factor of 28 at 850 ˚C, with the dispersion of nano-sized SDC particles on the surface of LSCM. This is ascribed to a much extended TPB compared to a bulk LSCM-SDC composite. The incorporation of SDC into LSCM matrix also provided an extra oxide ion conduction path besides faster surface reaction, which consequently enhanced anode activity towards H_2 oxidation.

An LSCM based anode was reported to benefit significantly from infiltration of multiple components with diverse functionalities. With multiple infiltrations of GDC (50 wt%) and Pd (0.5 wt%) into LSCM scaffold, comparable performance with a well-engineered Ni-cermet in a high temperature CO_2 electrolyser has been reported by Yue et al.[121] High temperature was necessary to attach a pure LSCM electrode to the dense YSZ electrolyte, thus interfacial contact is often a concern for LSCM based scaffold anode. A porous YSZ interlayer between the electrolyte and LSCM scaffold was found effective to improve contact between electrolyte and LSCM scaffold.

3.2.2 Perovskite LST based scaffold

Doped strontium titanates have been widely investigated as potential SOFC anode scaffolds, owing to their high conductivity, robustness in hydrocarbon fuels and good compatibility with YSZ electrolyte.[112,122,123] By doping at either A site or B site and by varying the stoichiometry, the properties of these n-type, electronically conducting materials can be tuned to improve their electrochemical activity.[124],[125] However, the electro-catalytic properties of these materials tends to be insufficient, so impregnation with active catalyst, such as doped ceria and/or Ni, is an effective strategy to boost the performance of strontium titanate anode.

When appropriately reduced lanthanum doped $SrTiO_3$ (LST) shows good electronic conductivity, which is promising as a conducting scaffold for impregnated anode systems. In particular the 10% A-site deficient $La_{0.20}Sr_{0.25}Ca_{0.45}TiO_3$ ($LSCT_{A-}$) can exhibit a conductivity of 28-30 S cm^{-1} at 900 ˚C.[126] The addition of the calcium also improves the sinterability of the material, and by careful control of particle morphology, allows a well bonded grain structure to be obtained while maintaining adequate porosity for gas transport functions. One of the advantages of the conducting scaffold is that the catalyst phase can be kept to a minimum, usually less than 5 wt%, which minimises any risks of physical damage on redox cycling even if utilising Ni.

Irvine et al. have carried out extensive studies on infiltration into the A-site deficient $La_{0.2}Sr_{0.25}Ca_{0.45}TiO_3$ ($LSCT_{A-}$) anode SOFC, testing with H_2 as well as CH_4.[112,127,128,129,130] With impregnated ceria (6-10 wt%) and Ni (3-5 wt%), a dramatic enhancement in anode performance was obtained compared to that of the bare $LSCT_{A-}$ backbone and the backbone with ceria only.[127] As shown in Figure 7, the performance enhancement mainly comes from a major decrease in the magnitude of the low frequency arc. When infiltrated with a mixture of Ni and CeO_2, cells showed electrochemical performances on par with conventional Ni-YSZ cermets, excellent redox stability of over 20 cycles, and long term durability. The microstructure analysis of the ceria-Ni impregnated $LSCT_{A-}$ anode both after testing at 900 ˚C for ~80 hrs and that of a cell after 20 redox cycles revealed

the presence of Ni particles of 50-100 nm size, whereas the cell with only Ni decorated $LSCT_{A-}$ anode showed performance that suffered from severe degradation due to sintering of the Ni particles. The tailoring of the electro-catalytic properties of $LSCT_{A-}$ anode by combined ceria and Ni infiltration was also demonstrated in a thick anode supported structure fabricated by aqueous tape casting, where 6% ceria and 4% Ni were coated on a 450 µm thick porous $LSCT_{A-}$ anode (pre-reduced at 1000 ˚C. A max power density of 960 mW cm^{-2} was obtained on testing in H_2 fuel at 800 ˚C.[129] These used a mixture of $LSCT_{A-}$ powders that were pre-fired at different temperatures to provide a matched thermal expansion in the scaffold with YSZ electrolyte.

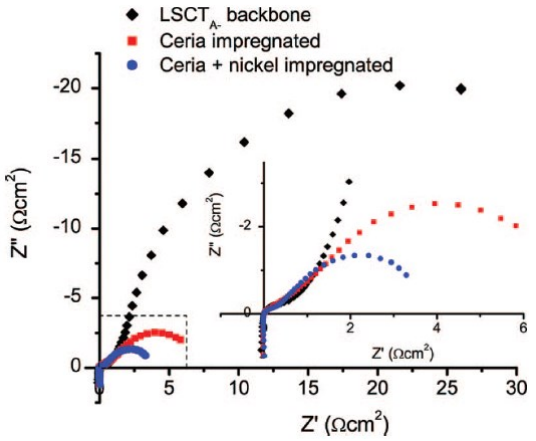

Figure 7 Cell impedance from $LSCT_{A-}$ backbone with either 10 wt% CeO_2 or with 10 wt% CeO_2 + 5 wt% Ni at 900 ˚C in H_2 with 1% H_2O at OCV. Reprinted with permission from J. Electrochem. Soc. 2012, 159, F757. Copyright 2012 The Electrochemical Society.

One aspect observed from the $LSCT_{A-}$ anode, from the studies mentioned above, was variations in the anode behaviour depending on the precise mix of catalysts used, specifically how the Ni interacted in the presence of either CeO_2 or GDC, both in terms of reduction kinetics and the final morphology of the catalysts. This again points to potential effects of variations in the surface energies of the different oxides present in the system. This will affect wetting and other interfacial properties, which strongly influence performance. This further underlines the importance of understanding these mechanisms and a great deal of the effort in this work has focussed on these aspects as a means to optimise the performance of infiltrated electrode systems.

Sasaki et al. utilized a 30 µm thick 40 wt% $(ZrO_2)_{0.89}(Sc_2O_3)_{0.1}(CeO_2)_{0.01}$-$La_{0.1}Sr_{0.9}TiO_3$ (SSZ-LST) functional layer and a LST layer as anode backbone to incorporate $Ce_{0.9}Gd_{0.1}O_2$ nano-structured catalyst.[131] With a maximum GDC loading (15 mg cm^{-2}), the anode overpotential was lowered appreciably in comparison to the anode without GDC particles. The cell voltage was 0.865 V at 200 mA cm^{-2} using a 200 µm thick SSZ electrolyte and a LSM-SSZ cathode in 3% H_2O-H_2 at 800 ˚C, and it was further promoted to over 0.97 V under identical conditions when 0.03 mg cm^{-2} Pd or Ni co-catalyst was introduced. It was stated that the presence of Pd or Ni nanoparticles strongly promote the reducibility of ceria through hydrogen spillover mechanism and the oxygen chemisorption on Pd or Ni by oxygen spillover, which would facilitate the hydrogen adsorption/dissociation and hydrogen diffusion processes on the metal surface. Consequently, even a small amount of Pd or Ni located on highly-conductive GDC surface can substantially enhance the hydrogen oxidation reaction.
Ramos et al. evaluated the performance and long-term stability of the Ni/CGO and Ru/CGO co-infiltration into $Sr_{0.94}Ti_{0.9}Nb_{0.1}O_3$ (STN94) anode on 5x5 cm^2 ScSZ electrolyte supported SOFC with LSM/YSZ cathode.[132] Compared to STN94 anode with only CGO, the anode with dual M/CGO (M= Ru, Ni) impregnates offered higher initial performance attributed to catalytic benefits from the small amount of metal co-catalyst, with the Ru/CGO anode showed the best performance. Concerning the long-term durability, the Ru/CGO infiltrated cell exhibited the lowest degradation rate, 0.04 mV h^{-1},

and in contrast, the Ni/CGO impregnated cell showed the highest degradation rate, 0.5 mV h^{-1} at 850 ˚C in 50% H_2O/H_2. These indicate that the choice of metal controls both the extent and the way the metals interacts with CGO. More in depth fundamental studies are needed in this area.

As microstructural evolution is of fundamental importance to understand the electrochemical responses, a detailed microstructural investigation was performed on the Ni/CGO impregnated into a STN94/10 vol.% YSZ scaffold as an anode symmetrical cell, tested under various H_2O/H_2 conditions.[133] The NiO/CGO nanoparticles exist as fluorite structure in the as-infiltrated sample both after decomposition at 350 ˚C and after sintering in air at 850 ˚C for 2h, indicating a strong interaction between NiO and CGO nanoparticles as a result of mixed nickel nitrate and (Ce, Gd) nitrates solution infiltration. Reduction in a H_2/N_2 mixture after sintering at 850 ˚C led to the separation of Ni and CGO phases, due to the significant growth in Ni particles (from 5 to 50nm) with limited growth in CGO particles. Based on these observations, it is reasonable to keep the metal loading low to avoid serious agglomeration if it is not necessary for conductivity requirements.

3.3 Other types of scaffolds

With the development of low temperature SOFC (LT-SOFC), metal supported cells have been developed. Nielsen et al. reported the first detailed impedance characterization of a cermet based anode with Ni:GDC (10wt% Ni in GDC) infiltration in metal-supported SOFCs, and studied the influence of Ni content, the amount of infiltration, backbone composition, impedance evolution during start-up, as well as temperature effects, i. e. sintering of Ni:GDC nano particles.[134] It was found that the addition of a small amount of Ni not only greatly improves performance (the resistance associated with the surface reaction was lowered by a factor of 10, and activation energy decreased from 114 kJ mol^{-1} to 49 kJ mol on addition of Ni, shown in Figure 8), but also provided a Ni-GDC matrix in which sub-micron sized Ni particles were trapped in the GDC network which prevented Ni particles from further growth in the temperature range 650-1000 ˚C.

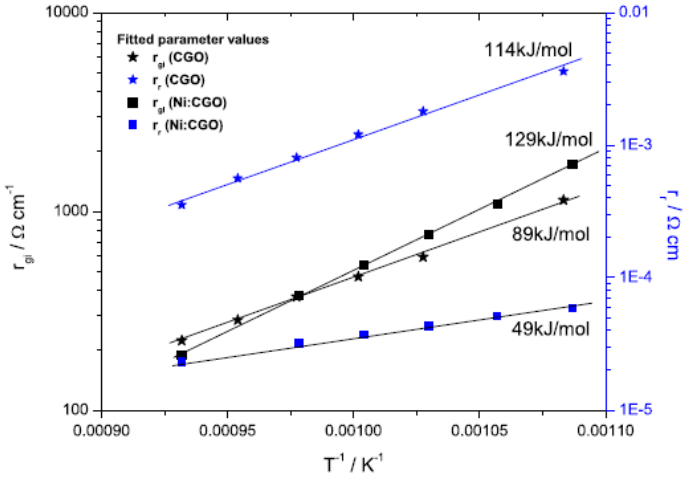

Figure 8 Arrhenius plot of the fitted impedance model parameters for CGO and Ni:CGO infiltrated anodes. Used with permission from Journal of Power Sources **2012**, 219, 305-316. Copyright 2012 Elsevier.

Spinel-structured $MnFeCrO_4$ was explored by Stefan et al. as scaffold for a range of materials to seek potential SOFC electrodes.[135] A symmetric cell design with $MnFeCrO_4|YSZ|MnFeCrO_4$ wafer was used, with the impregnates including LSCM, $La_{0.8}Sr_{0.2}FeO_3$ (LSF), GDC, CeO_2 and/or Pd, and were evaluated both in air as cathode and in humidified 5%H_2/Ar as anode. Substantial improvement in Rp with impregnation was observed, especially in air, though secondary phase presented in the composite with impregnated LSCM and that with LSF. However, significant deactivation in

$MnFeCrO_4$/LSCM/CeO_2 with and without Pd was observed with prolonged exposure (11 hour) to humidified 5%H_2/Ar at 850 ˚C, possibly due to ceria sintering and Pd passivation.

Perovskite-type (La,Sr)(Ga,Mg)O_3 (LSGM) has been widely applied as electrolyte material for LT-SOFC, due to its superior oxide ion conductivity over GDC and YSZ at the operating temperature of 500 - 650 ˚C. However, its reactivity with Ni during co-firing means the Ni-based cermet anode supported cell structure difficult to handle. Such a problem can be avoided by infiltrating Ni into the pre-fired LSGM frame. Barnett et al. successfully manufactured a LST anode supported LT-SOC with thin LSGM electrolyte from tape casting, with a $La_{0.6}Sr_{0.4}Co_{0.2}Fe_{0.8}O_3$ (LSCF)-GDC cathode from screen-printing, and with Ni impregnated into the anode.[136] The impregnation of Ni into the LST anode current collecting layer and LSGM anode functional layer (AFL) was optimised in terms of surface area, porosity, thickness of AFL as well as Ni loading. In the AFL with 30wt% pore former and 12.3 vol.% Ni, the estimated TPB length (calculated from quantitative analysis of 3D reconstruction with FIB-SEM) is ~6 times that of an Ni-YSZ anode supported cell fabrication from a typical co-firing.

Due to its excellent sulfur tolerance and superior redox properties in the intermediate temperature range, the double perovskite SFM has been of interest as alternative fuel electrode in SOCs.[105,137 138, 139, 140] As has been mentioned in section 3.1, the infiltration derived SFM-YSZ electrode displayed remarkable electrochemical performance and fair short-term stability, with avoided solid-state reactions between the two at temperatures lower than 1000 ˚C. When adopted as scaffold, impregnation with metal, such as Ni, was reported to be effective for enhancing the catalytic activity of SFM-based electrodes. On an LSGM electrolyte, Ni (2 wt%) impregnated SFM anode based cell showed much improved peak power density in wet H_2 at 800 ˚C compared to bare SFM anode cell (1.2 W cm^{-2} versus 0.7 W cm^{-2}).[140] Further, significant improvement in catalytic properties were also found from Ni impregnated SFM electrodes working in methane atmosphere.[139,140] Regarding sulfur tolerance, it was found that, due to the introduction of catalytically active Ni, significant degradation occurred when the impregnated Ni-SFM anode was exposed to H_2 with 100 ppm H_2S at 0.7V at 800 ˚C, however, this degradation was fully recovered upon removing H_2S.

4. Impregnated Cathodes

Similar to SOFC anodes there is considerable interest in preparing SOFC cathodes by infiltration techniques [141,142,143] and it can be argued that there is greater need to use this approach on the air electrode side due to the sensitivity to typical air electrodes to reaction with electrolyte or other skeletons at ceramic sintering temperatures

4.1 Infiltration of ion conductive phase

Infiltration of MIEC porous cathode with ion conductive promoters has been found to be an efficient way of creating morphologically altered electrode surface, extending the TPB density and increasing the surface area for ORR reaction[143]. It has also been shown to increase the oxygen exchange rate across the surface of the electrode[144] and so further increasing the ORR rate. Doped CeO_2 is routinely used as an ion conducting infiltrate material having higher coefficient of oxide ion conductivity than conventional cathode materials such as LSM and LSCF at intermediate SOFC temperatures [145] (see Figure 9).

The low ionic oxygen conductivity of LSM limits the ORR reaction to the areas close to TBP, hence infiltrating a phase with higher oxide ion conductivity was expected to lead to a significant performance improvement of LSM based cathodes. Jiang et al.[94] found that infiltrating LSM cathodes with GDC at loading levels of 5.8 mg cm^{-2} (~38 vol%) reduced the polarization resistance of the cathode drastically to 0.21 Ω cm^2 at 700 ˚C which made the performance of the GDC-impregnated LSM comparable to that of LSCF in the temperature range of 600–800 ˚C. An improvement factor

(F_{ASR} = ASR_{blank} / ASR_{inf}) was used as figure of merit accounting for the overall cathode polarization resistance reduction over the baseline "blank" cathode, where area specific resistances (ASR) of the blank electrodes (ASR_{blank}) and the infiltrated electrode (ASR_{inf}) were used as measurable variables. Whilst such improvement factors have some merit in evaluating enhancements due to the electrode treatment, they do not easily transfer between laboratories and are easily skewed if the "blank" runs are far from optimum, hence we try to focus on absolute values in this review. Such absolute values will tend to favour established materials that have had several years of optimisation but the intrinsic advantage of infiltration is that initial optimisation comes much easier than for bulk composites. Yoon et al.[146] achieved a slightly better performance for pure LSM cathode infiltrated with $Sm_{0.2}Ce_{0.8}O_2$ (SDC) yielding cathode polarization resistance of 0.19 Ω cm^2 at 700 ˚C. The effect of doped ceria infiltration was found to be more pronounced at lower temperatures (~650 ˚C) and for low-frequency responses related to the dissociation and diffusion of oxygen on the LSM electrode surface[147] . Similar electrochemical activity enhancement has been reported by several authors on LSM–YSZ composite cathodes infiltrated with doped ceria[142,148,149,150,151,152]. The effect of ionic conductive oxide infiltration at sufficient loading levels has been suggested to be related to the extension of TPB creating an ionic conducting path on top of the LSM particles and on top of the insulating low conducting zirconates at the LSM–YSZ interface [148] both of which enlarged the electrochemically active portion of the electrode. At the same time non-percolative nano structuring of the electrode surface was also shown to have substantial effect. Jiang et al.[147] reported that low loading level of GDC (~0.72 mg cm^{-2}; 3.1 vol%) can produce enhancement in electrochemical activity, despite GDC nano particles not forming ionic percolating phase. Ding et al.[153] used $Sm_{0.2}Ce_{0.8}O_{3-\partial}$ to decorate SDC nanoparticles on a $LaNi_{0.6}Fe_{0.4}O_{3-\partial}$ (LNF) cathode which appeared more tolerant towards Cr poisoning originating from the stainless steel interconnects than conventional LSM. Infiltration of composite cathodes with oxides that have a wide ranging ion conductivities and catalytic activities (CeO_2, SDC, YSZ, CaO[142] , Sm_2O_3[151]) have been shown to produce cathode performance improvements. These observations suggest that the oxide infiltrations cause additional effects such as scavenging of impurities as well as beneficial surface microstructural or chemical modification of the cathode scaffold itself.

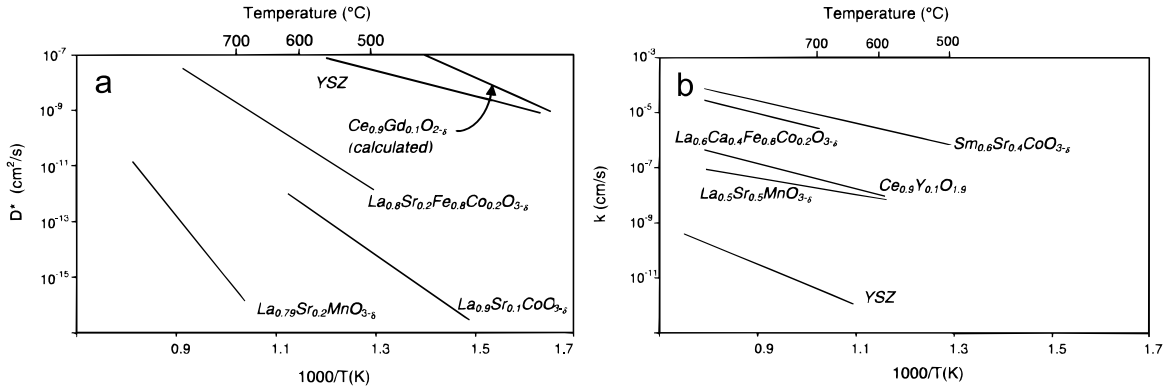

Figure 9 Diffusion coefficient (D*) (a) and Surface exchange coefficient (k) (b) for various cathode and electrolyte materials. Reproduced with permission from J. Electrochem. Soc., **1999** 146 (4) 1273. Copyright 1999 The Electrochemical Society.

Further reduction of the operating temperature of SOFCs to ~500 ˚C have been expected to allow widespread commercialization of SOFC (e.g. in the household sector for CHP application as well as direct utilization of commercially attractive fuels such as liquid methanol). The appraisals of doped ceria by Steele[154] have shown that ceria can maintain predominant ionic conducting in a reducing environment at low temperature. Hence, there has been a sustained development activity on high-performance cathodes for low temperatures application. LSCF is the preferred cathode material at low operating temperatures due to its high electronic conductivity (~340 S cm^{-1} at 550 ˚C [155]), high

ionic conductivity (~1x10^{-1} S cm^{-1} at 800 ˚C [156] in air), lower TEC value (14-15.3×10^{-6} K^{-1} at 373 - 873 K)[155], high surface exchange coefficient (k) and bulk diffusion (D*) coefficient (see Figure 9) [94,145] . A fundamental disadvantage of LSCF is its low structural stability. LSCF based cathodes were found to suffer from substantial long-term degradation, typically at a rate of 0.05% per hour[157,158]. Strontium oxide surface segregation is often reported as a major degradation mechanism for LSCF-based cathodes. According to Ding et al.[157] the combined effects of reduced surface stress and smaller surface charge result in SrO-terminated surfaces having lower energy than LaO-terminated surfaces. The enrichment of SrO at the cathode surface causes deactivation of ORR sites and decrease in surface activity. Lowering the operational temperature is a straightforward way to slow down such degradation problems; however, the expected reduction of electro-catalytic activity needs to be counteracted by extending TPB density and minimizing the polarization losses. Introducing an ion conductive nano phase onto the LSCF scaffold via infiltration can enhance TPB length creating higher conduction oxide ion paths and improving the stability of the cathode. A number of studies have shown that the addition of doped ceria can also accelerate the oxygen surface exchange rate. Xia et al. [159,160,161] used electrical conductivity relaxation method and found that coating LSCF with Sm-doped ceria resulted in an increase by a factor of 10 in the surface exchange rates. The surface exchange coefficient of the SDC coated LSCF was found to be dependent on the conductivity of doped ceria providing additional free oxygen vacancies for the surface exchange reaction. It was suggested that the oxygen exchange process at LSCF/SDC/gas triple phase boundary sites was faster than that taking place on the pure LSCF surface. The infiltration of $Gd_{0.2}Ce_{0.8}O_2$ into screen printed $La_{0.8}Sr_{0.2}Co_{0.5}Fe_{0.5}O_{3-\delta}$ was reported by Chen et al.[162] to significantly reduce the polarization resistance values as compared to the pure LSCF cathode from 0.22 Ω cm^2 to 0.06 Ω cm^2 at 750 ˚C with 1.5 mg cm^{-2} CGO loading. Nie et al.[163] performed infiltration of tape-casted LSCF6428 cathodes with aqueous nitrate solutions of $Sm_{0.2}Ce_{0.8}O_{1.95}$ (SDC) precursors and glycine as a complexing agent. Impedance analysis of LSCF/SDC/8 mol% Y_2O_3-ZrO_2/SDC/LSCF symmetric cells indicated dramatically reduced polarization losses, from a blank cathode polarization resistance value of 0.15 Ω cm^2 to 0.074 Ω cm^2 for the infiltrated cathode at 750 ˚C. Enhanced performance and stability of LSCF cathodes were reported by Liu et al.[164] when $La_{0.4875}Ca_{0.0125}Ce_{0.5}O_{2-\delta}$ (LCC) was applied as a thin-film coating on the scaffold surface. When 5 µL of 0.25M LCC precursor was infiltrated into the LSCF cathode, the cathodic polarization resistance was reduced to 0.076 Ω cm^2 from 0.130 Ω cm^2 at 750 ˚C. An exception of this trend was the result reported by Zhao et al.[165] on the infiltration of one-dimensional $La_{0.8}Sr_{0.2}Co_{0.2}Fe_{0.8}O_{3-d}$ nanorod-based cathode infiltrated with $Ce_{0.8}Gd_{0.2}O_{1.9}$ precursor. A significantly greater reduction in the polarization resistance was reported, illustrating the importance of the cathode microstructure on the ink dispersion. The nanorod-based scaffold in this case provided optimized “one-dimensional” porosity allowing easier ink penetration and hence higher loading limit for the CGO precursor. Using single step inkjet printing infiltration of CGO in composite LSCF/CGO cathodes Tomov et al.[38] reported ASR of 0.17 Ω cm^2 measured at 650 ˚C. These values were achieved with very low expenditure of the ink by sequential infiltration of nL size drops with high lateral resolution in a single step infiltration procedure.

4.2 Infiltration of noble and transition metal promoters

Enhancing the cathode performance at low operational temperature can also be achieved by modification of the cathode scaffold with noble and transitional metal promoters. Introduction of both the noble metal promoters - Pd[162,166], Pt[167,168], Ag[167,169,170] and the low-cost transition metal promoters - Cu[171,172], Ni[173], Co[174] have been evaluated. The mechanism of metal promotion is not yet fully understood and a number of contradicting reports have been published citing both positive and negative promotion factors. The electro catalytic effect of metal promoters on oxygen adsorption-dissociation process and the higher surface area generated by infiltration of nano-particle decorations are often cited as the main contributions to the enhancement of ORR[175,176].

Improvements were generally more pronounced at lower operational temperatures (500-650 ˚C) indicating the potential benefit of cathode infiltration with metal promoters for reduced temperature SOFCs. The effect of metal promoters on SOFC cathode performance was found to be dependent on a complex balance between the enhanced oxygen adsorption/dissociation rate and the interfacial oxygen transfer rate, which could be influenced, in a different degree by the interaction of the metal phase in the MIEC cathode. Serra et al.[166] experimented with Pd impregnation in LSCF and found by XPS that approximately 20% of the Pd is present as metal and the rest exists in oxidised form, presumably incorporated into LSCF B-site. They reported that Pd substitution may accelerate the redox cycles of the charge carriers, $Co^{3+}/Co^{4+}$and Fe^{3+}/Fe^{4+}, at B-site, hence improving the reduction of oxygen atoms. Sakito et al. [169] reported enhancement of maximum output power density by 1.5 times by infiltration of $AgNO_3$ solutions into porous $La_{0.6}Sr_{0.4}Co_{0.2}Fe_{0.8}O_3$ electrodes. In a similar experiment, Huang et al. [167] infiltrated 2 wt.% of Pt, Ag (in metallic state) and Cu (as oxide) into composite LSCF-GDC cathode and found a promotion trend of Cu > Ag > Pt. As pointed out by the authors, the reactivity for O_2 dissociation over Pt was expected to be better than that of Cu and that of Ag worse than Cu. The discrepancy was assigned to the difference of the oxygen affinities of the metals used and the different influence of the metal promoters on the rate of oxygen transport from the metal surface into the oxygen vacancy in the LSCF lattice. Guo et al.[176] pointed out that the effect of metal promoter interaction with the lattice of the oxygen-ion conducting LSCF perovskite could be associated with the size of the metal cation in comparison with that of the A-site or B-site cation in the ABO_3 perovskite. The cation radius of Cu^{3+} (0.68 Å) is well matched to that of LSCF B-site Co^{3+} (0.685 Å) assuring good interaction of Cu with the LSCF lattice. The cation radius of Ag^{+} (1.29 Å) is close to that of the LSCF A-site La^{3+} (1.15 Å), also resulting in a good interaction of Ag with LSCF A-site cations. On the other hand the ionic radiuses of Pd^{4+} (0.755 Å) or Pt^{4+}cation (0.765 Å), does not provide as close match with LSCF B-site cations hence the surface interaction can cause local de-stabilization of LSCF lattice. While Sahibzada et al.[177] and Simmer et al.[178] observed positive promotion effect of Pd added to LSCF and LSF based cathodes, especially at lower operational temperatures, Haanappel et al.[179] found that neither infiltration of the cathode with Pd solution nor mixing with Pd black resulted in a positive effect. The explanation for these contradictory results could be related to other factors such as the distribution and the size of the promoters, lack of convention on the loading levels measure as well as the non-optimal calcination procedures. As illustrated by Guo et al.[176] the loading level of transitional metal oxides and noble metals has an optimum above which the interfacial oxygen transfer can be negatively influenced as the promoting nano particles start to obstruct the interaction sites of interfacial O with the cathode surface oxygen vacancies (See Figure **10**).

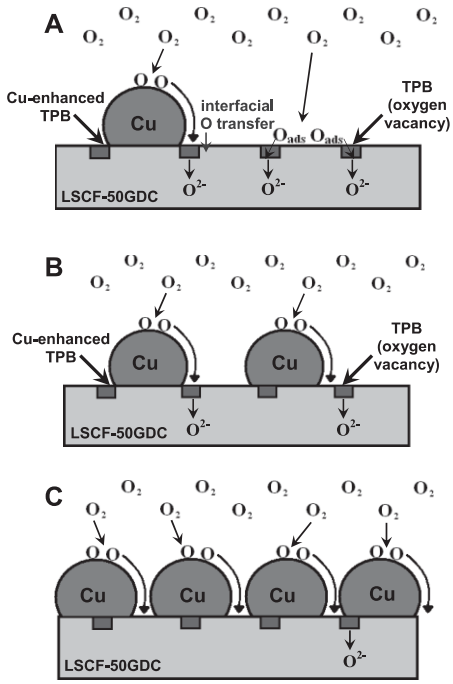

Figure 10 Schematic diagram of the Cu content on the electrochemical reaction of oxygen over the cathode TPB. The diagrams of a, b and c simulate LSCF-GDC doped with Cu, 1 wt%, 2wt% and 5wt.%, respectively. Reproduced with permission from *Fuel Cells* **2010**, *10*, 718. Copyright 2010, Wiley.

4.3 Durability of infiltrate cathodes

A general issue with ORR reaction enhancement via nano-decoration of the cathode surfaces is the inherent instability of nano-structured decorations which tend to agglomerate at operation temperatures due to the large surface energy associated with the nano-sized particles. A systematic comparative study on the stability of MeOx promoted ORR in LSCF based cathodes was performed by Gao et al.[180,181] (see Figure **11**a) using infiltration of metal nitrate salts (Cu, Ni, Co, Ag) dissolved in Ethanol with citric acid as additive. After an initial substantial reduction of the polarization resistance all infiltrated cathodes were found to deteriorate at different rates (V_d) with following the tendency V_d(LSCF+Cu) >> V_d(LSCF+Ni) > V_d(LSCF+Ag) = V_d(LSCF+Co)). After an initial period of accelerated coarsening leading to distinctively different morphological features, Ag and Co infiltrated samples reached stabilization of ASR values after approximately 100 hours of testing. In comparison, ASR values of Cu and Ni infiltrated polarization resistances were still increasing after 150 hours of testing. While Ag and Co tended to agglomerate at the grain boundaries of the composite LSCF/CGO cathode and likely act as inhibitors in the scaffold grains sintering process, the infiltrated Cu and Ni nano particles were observed to be randomly distributed on the scaffold surface with Cu particles agglomeration significantly larger and non-uniform in size (see Figure **11** b-e).

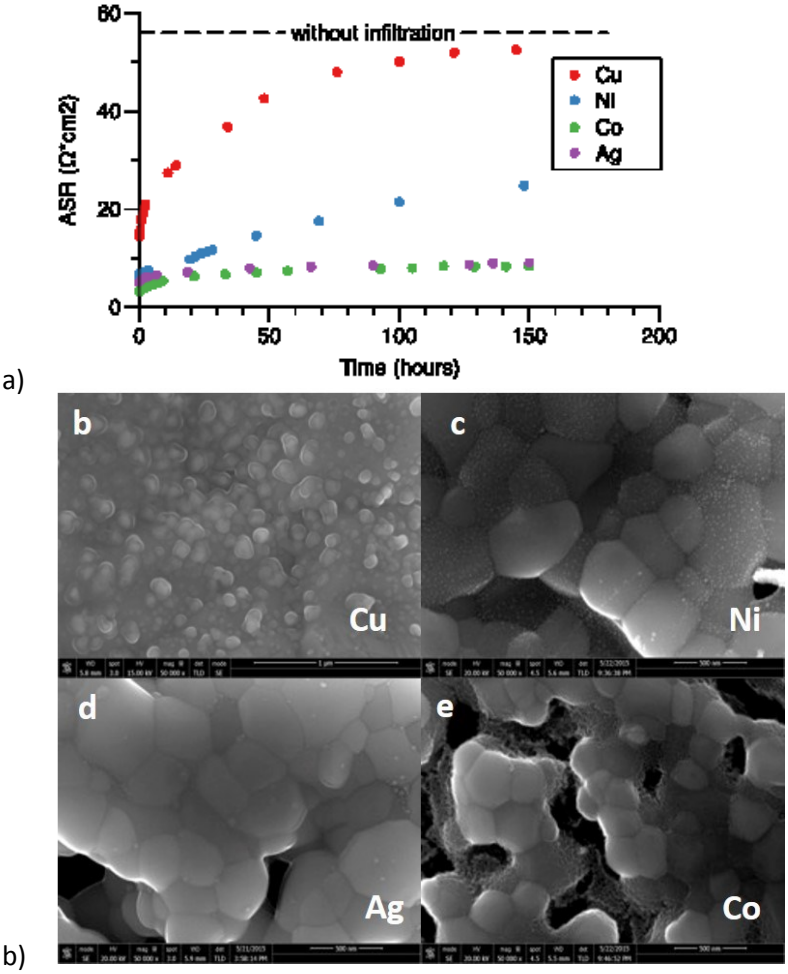

Figure 11 Ageing behaviour of LSCF/CGO cathodes infiltrated with Cu, Ni, Ag and Co promoters – (a) ASR vs aging time at 500 °C in air, (b-e) SEM of infiltrated LSCF/CGO cathodes after 150 hours aging [180,181].

The use of $Pr_{0.75}Sr_{0.2}MnO_{3-\delta}$ (PSM) and $PrSrCoMnO_{6-\delta}$ (PSCM) impregnates on LSFC scaffolds[182] showed improved performance and enhanced durability compared to the bare LSCF electrode. The chemical interdiffusion between the impregnate and the scaffold was observed by Raman

spectroscopy. This may give a mechanism to reduce the Sr segregation, which leads to cell degradation.

Application of sintering inhibitors infiltrated in a dual infiltration sequence was explored by various groups as a method to alleviate deterioration of infiltrated nano-sized promoters and to prolong the lifetime of the cell. Strong metal support interactions of sintering inhibitors (e.g., MgO, Al_2O_3, TiO_2, ZrO_2, CeO_2, $Ce_{0.9}Gd_{0.10}O_{1.95}$) has been utilised to prevent the coarsening of metal promoter nanoparticles. Co distributed inhibitor nano particles separated the catalyst particles effectively preventing their coalescence. Recently, Burye et al.[183] reported reduction of the cathode's polarization resistance to 0.1 Ω cm^2 at 540 ˚C and stable performance of the as-prepared cathodes by dual sequential infiltration of CGO and LSCF inks into a CGO porous scaffold. Imanishi et al. [152] reported that dual infiltration of $Co(NO_3)_2$ and $Ce(NO_3)_3$ in LSM-YSZ cathode improved the catalytic activity of the LSM-YSZ cathode and suppressed the aggregation of the fine particles of Co_3O_4. No significant degradation of the catalytic activity of the Co_3O_4 and CeO_2 co-infiltrated LSM-YSZ electrode was observed at 800 °C for 100 h. Wang et al. [184] enhanced the electrochemical performance of LSM/8YSZ with co-infiltration of PdO and ZrO_2 (Pd/Zr = 0.8/0.2). It was observed that uniformly deposited PdO particles were surrounded by nano-sized ZrO_2 particles. This distinctive microstructure was found to hinder the agglomeration and growth of PdO particles. As a result, the electrocatalytic activity of the cathode was enhanced and fully stabilized at the level of 0.36 Ω cm^2, after current polarization at 750 ˚C under 400 mA cm^{-2} for 200 h. The same enhanced durability over 4000 h has also been shown using Atomic Layer Deposition to coat a very thin layer of ZnO over impregnated $La_{0.6}Sr_{0.4}CoO_{3-\delta}$ particles[185]. The durability was attributed to confining thermal growth of the nanoparticles, and suppressing surface Sr-segregation.

5. Scale-up and Outlook

Impregnation is well suited to large scale cell manufacture and especially to modification of standard cells; however, there have been only limited reports of successful large cell manufacture using impregnation techniques.

Work relevant to scaling up of the impregnation technique focuses on engineering the YSZ wafer structure *via* cost-effective tape casting procedures or combination of tape casting and screen-printing.[186, 187]Cassidy et al.[186] have looked into SOFCRoll design with YSZ scaffold produced by sequential tape casting and a single co-firing step. As illustrated in Figure **12**(a), the SOFCRoll concept is a novel hybrid design of planar and tubular geometry based on a double spiral form, which could combine the advantages of both planar and tubular designs. The sequential tape casting was found to be able to produce a triple cast structure with a dense YSZ electrolyte sandwiched between two porous YSZ scaffolds, which eliminated detrimental defects, such as cracks, delamination etc., from stresses induced by separately cast layers. It was realised that the type of pore former and casting sequence impacted significantly on the following impregnation steps, e.g. by changing the surface wetting characteristics. With an optimised formulation, well cast triple layer tapes (Figure **12**(b)) were created and proved to be robust, with reasonable handle-ability in the green state, for further processing and rolling operations.

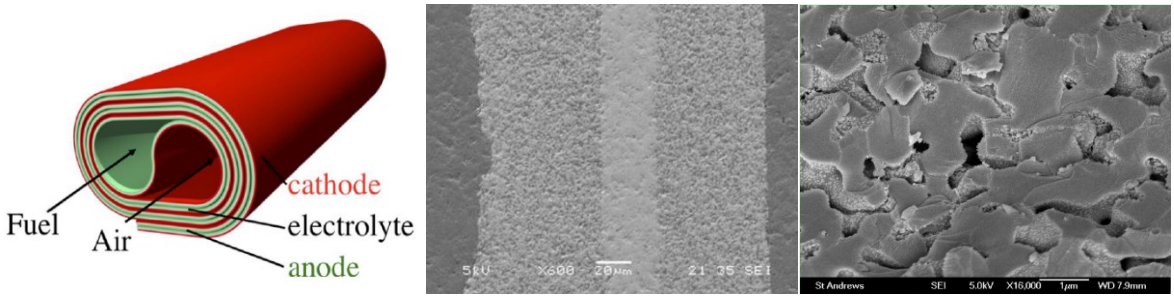

Figure 12 (a) Schematic geometry of SOFCRoll design, (b) Cross-sectional view of triple cast YSZ layer produced by sequential casting before infiltration, and (c) micrograph showing impregnates catalyst on the pore surface of SOFCRoll support **186**

One of the big issues with scaleup is the production of suitable scaffolds, with the required surface properties and porosity to impregnate properly. This has been investigated by Cassidy et al.[187] using an aqueous tape casting technique and employing other fugitive pore formers, including acrylic microspheres and starch. A variety of porous YSZ structures were created by using rice starch, 8 µm PMMA, and 35-45 µm PEMA either separately or combined to produce a porous scaffold suitable for subsequent infiltration.

An attempt to transfer developed ceramic formulations and methods in the lab to an industrial relevant level with novel ceramic materials has been reported recently on aqueous tape casting and subsequent infiltration.[188] Anode supported half cells were successfully manufactured by aqueous tape casting and infiltration, where $LSCT_{A-}$ was the supporting scaffold for infiltration with different types of ceria impregnated. Challenges remain regarding the level of sufficient porosity, expanding porosity with proper pore formers if needed, as well as how porosity impacts microstructure, electrode electronic conductivity and mechanical stability especially in operating conditions.

In one exemplification, electrolyte supported cells with conventional LSM based cathodes and $LSCT_{A-}$ titanate perovskite anode skeletons were fabricated via screen printing. The anodes of the resulting cells were then infiltrated with appropriate electrocatalysts and the resulting SOFC cells formed into stacks. Trials were carried out using Ni mixed with either CeO_2 or GDC infiltrates in commercial scale cells and short stacks (Hexis AG) which culminated in a demonstration of the impregnated $LSCT_{A-}$ anodes in a kW level full size stack (Hexis Galileo System) which achieved power output of 750W running on CPOx (catalytic partial oxidation) reformed natural gas.[128] This has proven the feasibility of up-scaling with infiltration into $LSCT_{A-}$ anode. The 5-cell short stack (each cell has an active area of 100 cm^2) with ceria and Ni co-infiltrated $LSCT_{A-}$ exhibited comparable performance to the standard HEXIS Ni-cermet based anode. However, durability testing showed heavy degradation over 1000 hrs whilst running at 200 mA cm^{-2} at 900 ˚C in CPOx reformed natural gas, whereas the short stack with GDC and Ni infiltrated $LSCT_{A-}$ anode displayed much improved durability in similar operating conditions, except that it was run at 850 ˚C to avoid sintering of nanoparticles (Figure 13). However, as shown in Figure 14, the durability of the Ni and GDC impregnated $LSCT_{A-}$ anode did not sustain in the kW scale stack test running at a gas input of 3.3 kW and constant stack voltage at an average temperature of 850 ˚C. The degradation was most severe in the central clusters of the stack, with a drop in the voltage from 700 mV to 300mV observed in the most centrally positioned cluster whilst a temperature gradient observed across stack with the central clusters exhibiting temperature of up to 100 ˚C higher than other clusters. The degradation mechanism was not clear, however, the Ni/GDC cells had very thin $LSCT_{A-}$ backbone (10-15 µm) with relatively dense microstructures due to some processing issues during scaling-up process, which might affect the current collection in Ni/GDC cells in the large scale stack.

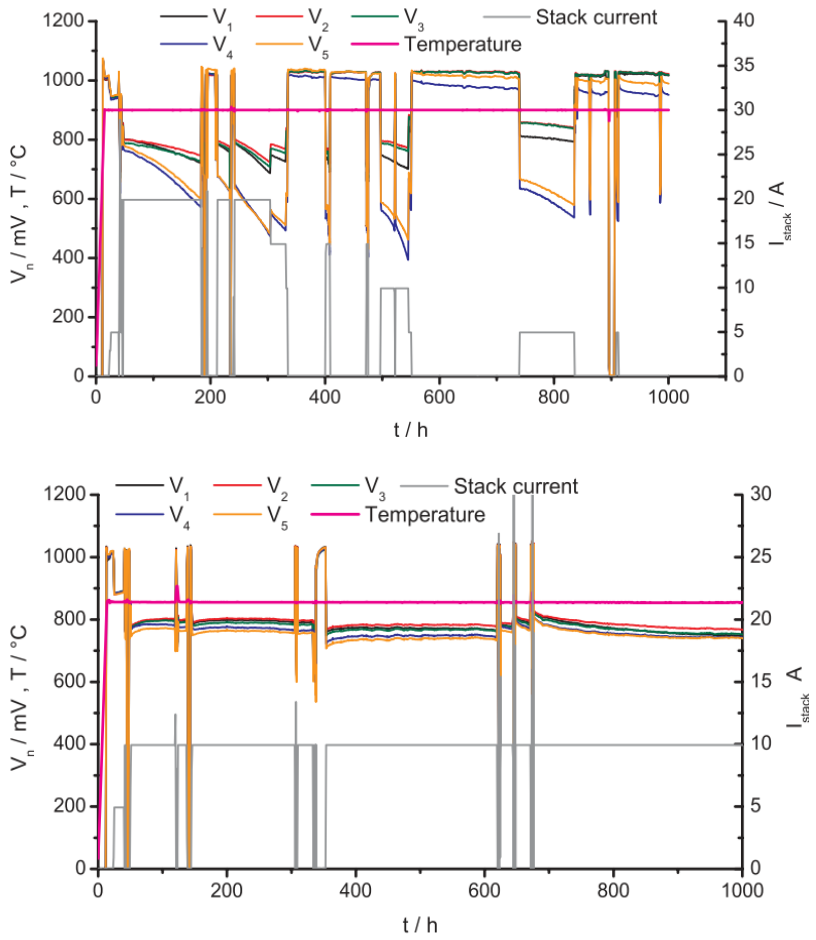

Figure 13 Stability tests of 5 cell stack with $LSCT_{A-}$ anode with $Ni+CeO_2$ as impregnated catalysts at 900 ˚C in 4 g h^{-1} of CPOx (catalytic partial oxidation) reformed natural gas (a) and that with Ni + GDC as impregnated catalysts at 850 ˚C (b) in the identical gas conditions. Reproduced with permission from Fuel Cells 2015**, 15, 682.** Copyright 2015 Wiley.

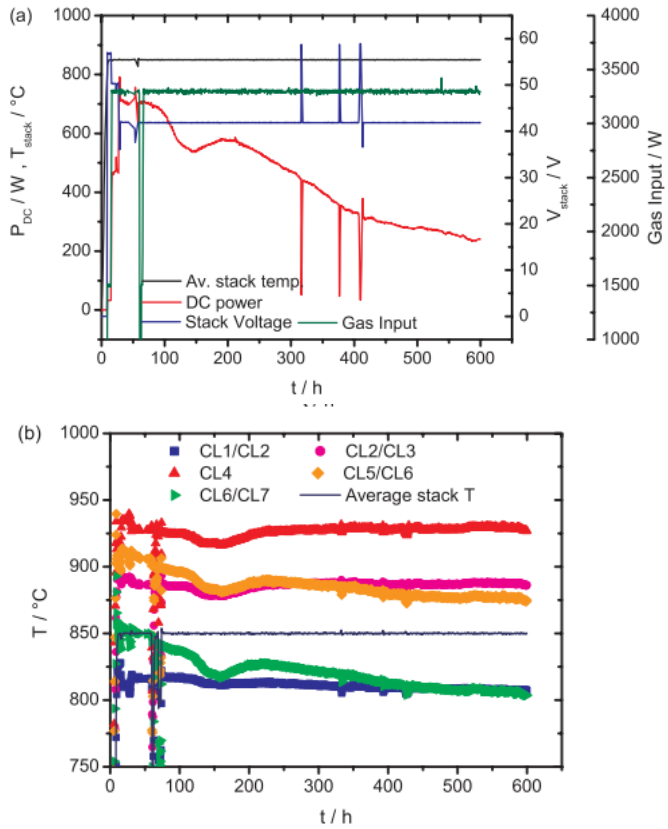

Figure 14. Results from Hexis Galileo system test with $LSCT_{A-}$ anodes impregnated with Ni + GDC (a), and monitored Cluster temperatures during test (b) which shows large thermal gradient across stack, with central clusters (CL3, CL4, CL5) displaying temperatures up to 100 ˚C higher than external clusters (CL1 and CL7). Reproduced with permission **from Fuel Cells** 2015**, 15, 682. Copyright 2015 Wiley.**

Whilst the above discussion of large scale, commercially relevant cells, involved only half cell impregnation, other reports relate to impregnation of preformed skeletons for both anode and cathode. The feasibility of fabricating large-area planar cells with nano-structured electrodes has been demonstrated with YSZ scaffold.[189] A 5x5 cm flat tri-layer YSZ scaffold was manufactured via cost-effective tape casting by Ni et al. and precursor solutions of $La_{0.8}Sr_{0.2}FeO_3$ (LSF) and $La_{0.7}Sr_{0.3}VO_{4-\delta}$ (LSV_{ox}) were impregnated into the porous YSZ scaffold as cathode and anode, respectively and then fired at 900 ˚C. The maximum power output of the cell with additional 10 wt% CeO_2 and 1 wt% Pd co-impregnated on the anode were 300 mW cm^{-2} and 489 mW cm^{-2} at 700 °C and 800 °C respectively, with humidified H_2 (4.2 vol% H_2O) as fuel and air as oxidant, which gave a maximum power of 6 W for a single cell at 800 °C, Figure **15**.

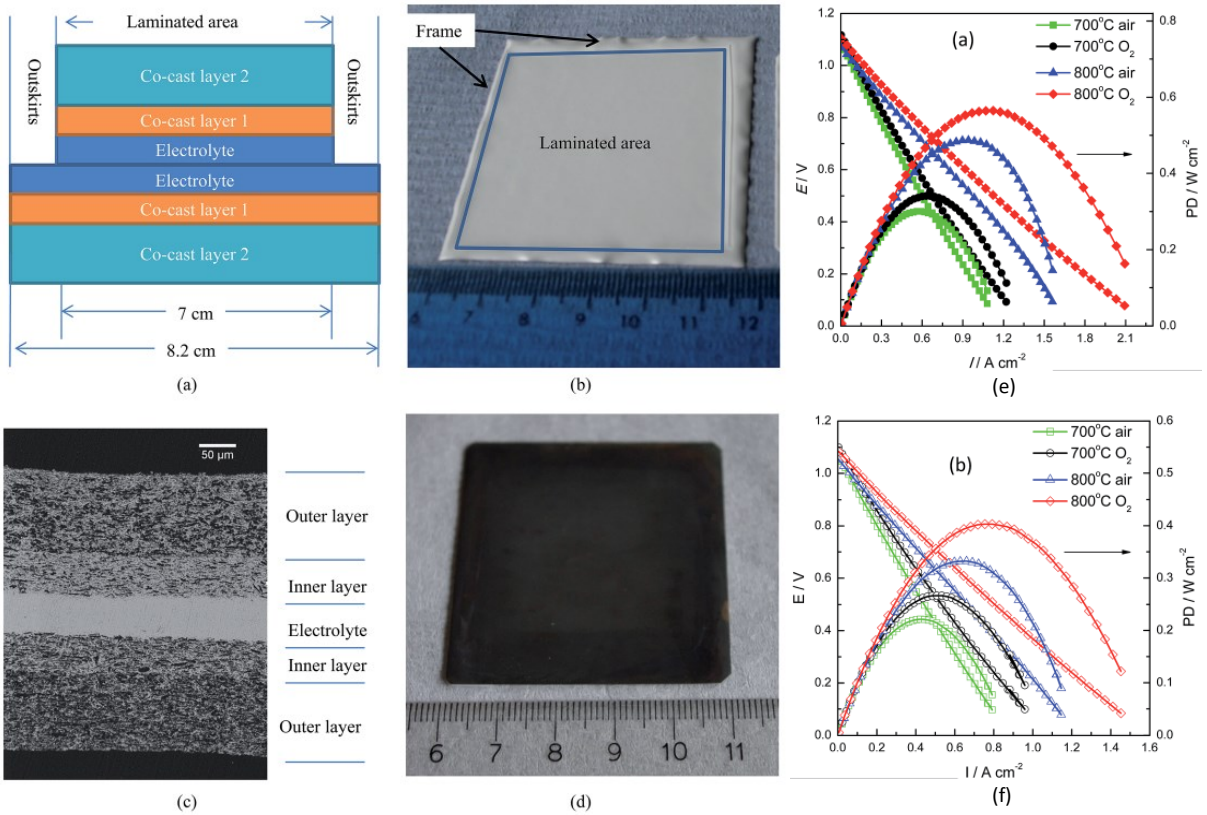

Figure 15 (a) Schematic illustration of the lamination of the YSZ green tapes with two co-cast layers containing YSZ and varied amounts of graphite; (b) the scaffold sintered at 1400 ˚C having a flat laminated area and a warping frame from the outskirts of green tapes; (c) The SEM cross-section of the scaffold with a dense electrolyte and two identical gradient porous structures for the electrodes; (d) the image of the fuel cell (cathode side) after impregnation and scraping off the frame; Performance of the fuel cell with ceria + Pd as a catalyst under air or oxygen as an oxidant before (e) and after (f) a redox cycle at 900 ˚C *Adapted from J. Mater. Chem. A*, 2014, *2*, 19150, Copyright 2014, by permission of The Royal Society of Chemistry.

Topsoe Fuel Cells have looked at impregnation on the stack level to help the performance and durability of its stacks. They used standard cell impregnation methods to improve cathodes[190]. They did multiple impregnation steps and followed the amount of added material, and then looked at both the microstructure and in-plane electrode resistance, to correlate with cell performance. The impregnated cell performance was stable over 250 h of testing at 700 ˚C but did show a loss of electrode resistance at high temperature due to sintering behaviour of the impregnate.

They also investigated whether finished stacks could be impregnated[191] once assembled. They used two stacks, and tested them before and after impregnation with CGO on the cathode and Ni/CGO on the anode side. The tested stack gave more porosity in the reduced NiO/YSZ anode for better impregnation. The impregnations of the stack were successful showing improvement for both OCV and cell voltage under load. The cells were checked post-mortem by electron microscopy to show the morphology and elemental distribution of the cells.

Conclusion

It has been clearly shown that the impregnation of electroactive species into a porous framework can produce electrodes comparable in performance to state of the art (bulk) electrodes, while removing some of the problems of existing electrodes production and long term operation. Impregnation is a very flexible technique, with applications for both cathodes and anodes, and with

the ability to add one or more of the catalytic, ionic and electronic conducting phases. The ability to add these phases in small amounts to the important surfaces in an electrode makes this a powerful and cost effective method. The fact that the method works is clear, but the basic science behind the both the interactions during the impregnation itself, with the liquid-solid and solid-solid wetting, and the catalytic integrations between the impregnated species is still poorly studied and understood. There needs to be increased studies of the basics of the process, such as wetting, and chemical interactions during formation and operation to couple with and understand better the engineering of this very useful technique for electrode modification.

Acknowledgements
We thank EPSRC for support through the research grant EP/M014304/1

References

1 M. Cassidy, K. Kendall, G. Lindsay, *J. Power Sources*, **1996**, 61, 189.
2 D. Sarantaridis, A. Atkinson, *Fuel Cells*, **2007**, 7, 246.
3 M.L. Toebes, J. H. Bitter, A. J. van Dillen, K. P. de Jong, *Catal. Today*, **2002**, 76, 33.
4 Y. Matsuzaki, I. Yasuda, *Solid State Ionics*, **2000**, 132, 261.
5 A. Barbucci, M. Viviani, M. Panizza, M. Delucchi, G. Cerisola, *J. Appl. Electrochem.*, **2005**, 35, 399.
6 J. A. Kilner, M. Burriel, *Annual Rev. Mater. Res.* **2014**, 44, 365.
7 C. Sun, R. Hui, J. Roller, *J. Solid State Electrochem.*, **2010**, 14, 1125.
8 A. Lashtabeg, S. J. Skinner, *J. Mater. Chem.*, **2006**, 16, 3161.
9 H. Uchida, S. Arisaka, M. Watanabe, *Electrochem. Solid-State Lett.,* **1999**, 2, 428.
10 Z. Liu, B. Liu, D. Ding, M. Liu, F. Chen, C. Xia, *J.Power Sources*, **2013,** *237*, 243
11 T. Z. Sholklapper, H. Kurokawa, C.P. Jacobson, S.J. Visco, L.C.De Jonghe, *Nano Lett*., **2007,** 7, 2136.
12 D.A. Osinkin, N.M. Bogdanovich, S.M. Beresnev, V.D. Zhuravlev *J. Power Sources*, **2015**, 288, 20.
13 J.T.S. Irvine, D. Neagu, M. C. Verbraeken, C. Chatzichristodoulou, C. Graves, M. B. Mogensen, *Nat. Energy*, **2016**, 1, 1.
14 R. Craciun, S. Park, R. J. Gorte, J. M. Vohs,a C. Wang, W. L. Worrell, *J. Electrochem. Soc.*, **1999**, 146, 4019.
15 S. Jung, C. Lu, H. He, K. Ahn, R.J. Gorte, J.M. Vohs, *J. Power Sources*, **2006**, 154, 42.
16 E. N. Hodkin, M. G. Nicholas, *J. Nucl. Mater.,* **1973**, 47, 23.
17 P. Nikolopoulos, S. Nazare, F. Thümmler, *J. Nucl. Mater.,* **1977**, 71, 89.
18 P. Nikolopoulos, *J. Mater. Sci.,* **1985**, 20, 3993.
19 D. Sotiropoulou, P. Nikolopoulos, *J. Mater. Sci.,* **1991**, 26, 1395.
20 A. Tsoga, P. Nikolopoulos, *J. Mater. Sci.,* **1996**, 31, 5409.
21 D. Reed, G. Coffey, E. Mast, N. Canfield, J. Mansurov, X. Lu, V. Sprenkle, *J. Power Sources*, **2013**, 227, 94.
22 F. Peng, Y. Li, P. Nash, J. F. Cooper, S. J. Parulekar, J. R. Selman, *Int. J. Hydrogen energy*, **2016**, 41, 18858.
23 R. Trejo, E. Lara-Curzio, A. Shyam, M. J. Kirkham, V. Garcia-Negron, Y. L. Wang, *Int. J. Appl. Glass Sci.*, **2012**, 3, 369.
24 L. Rezazadeh, Z. Hamnabard, S. Baghshahi, A. N. Golikand, *Ionics*, **2016**, 22, 1899.
25 J. Hao, Q. Zan, D. Ai, J. Ma, C. Deng, J. Xu, *J. Power Sources*, **2012**, 214, 75.
26 R. Chatzimichail, G. Triantafyllou, F. Tietz, P. Nikolopoulos, *J. Mater. Sci.*, **2014**, 49, 300.
27 T. Gambaryan-Roisman, *Curr. Opin. Colloid Interface Sci.*, **2014**, 19, 320.
28 X. Lou, Z. Liu, S. Wang, Y. Xiu, C. Wong, M. Liu *J. Power Sources*, **2010**, 195, 419.
29 C. Knöfel, H. Wang, K. T. S. Thydén, M. Mogensen, *Solid State Ionics*, **2011**, 195, 36.
30 K. K. Hansen, M. Wandel, Y. L. Liu, M. Mogensen, *Electrochim. Acta*, **2010**, 55, 4606.
31 N. S. Xu, X. Li, X. Zhao, H. L. Zhao, K. Huang, *Electrochem. Solid-State Lett.*, **2012**, 15, B1.
32 K.S. Howe, A.R. Hanifi, K. Kendall, Mark Zazulak, T.H. Etsell, P. Sarkar, *Int. J. Hydrogen Energy*, **2013**, 38, 1058.
33 C. Savaniu, D.N. Miller J.T.S. Irvine, *J. Am Ceram. Soc.*, **2013**, 96, 1718.
34 A. Buyukaksoy, V. Petrovsky, F. Dogan, *J. Electrochem. Soc.*, **2012**, 159, B666.
35 R. Kiebach, C. Knöfel, F. Bozza, T. Klemensø, C. Chatzichristodoulou, *J. Power Sources*, **2013**, 228, 170.
36 X. Lou, S. Wang, Z. Liu, L. Yang, M. Liu, *Solid State Ionics*, **2009**, 180, 1285.
37 J. Choi, W. Qin, M. Liu, M. Liu, *J. Am. Ceram. Soc.*, 2011, **94**, 3340.
38 R. I. Tomov, T. Mitchell-Williams, C. Gao, R. V. Kumar, B. A. Glowacki, *J. Appl. Electrochem.*, **2017**, 47, 641.
39 N. Zouvelou, X. Mantzouris and P. Nikolopoulos, *Mater. Sci. Eng.: A.,* **2008***,* 495, 54.
40 T. Inoue, H. Matzke, *J. Am Ceram. Soc.*, **1981**, 64, 35.
41 R. H. Bruce, in: *Science of Ceramics*, Vol. 2, (ed. G. H. Stewart), Academic Press, London **1965.**
42 G. Triantafyllou, G. Angelopoulos, P. Nikolopoulos, *J. Mater. Sci.,* **2010**, 45, 2015.
43 D. K. Owens, R. C. Wendt, *J. Appl. Polym. Sci.,* **1969**, 13, 1741.
44 P. Nikolopoulos, S. Agathopoulos, *J. Eur. Ceram. Soc.,* **1992**, 10, 415.
45 F. Fowkes, *Ind. Eng. Chem.,* **1964**, 56, 40.
46 S. Agathopoulos, M. Nedea, B. Ghiban, J. Ferreira, P. Nikolopoulos, *Key Eng. Mater.,* **2005**, 284, 1023.
47 C. Jie-Rong, W. Xue-Yan, W. Tomiji, *J. Appl. Polym. Sci.,* **1999**, 72, 1327.
48 A. Tsoga, P. Nikolopoulos, *J. Mater. Sci.,* **1996**, *31*, 5409.
49 X. Mantzouris, N. Zouvelou, D. Skarmoutsos, P. Nikolopoulos, F. Tietz, *J. Mater. Sci.*, **2005**, 40, 2471.
50 X. Mantzouris, N. Zouvelou, V. A. C. Haanappel, F. Tietz, P. Nikolopoulos, *J. Mater. Sci.*, **2007**, 42, 10152.
51 Y.-W. Choi, H. Mistry, B.Roldan Cuenya *Current Opinion in Electrochemistry,* **2017**, 1, 95

[52] J.D.Kirtley, S.N.Qadri, D.A.Steinhurst, J.C. Owrutsky, *J. Power Sources*, **2016**, 336, 54
[53] D.A. Agarkov, I.N. Burmistrov, F.M. Tsybrov, I.I. Tartakovskii, V.V. Kharton, S.I. Bredikhin, *Solid State Ionics* **2017**, 302, 133
[54] J. S. Hardy, J.W. Templeton, D.J. Edwards, Z. Lu, J. W.Stevenson *J. Power Sources* **2012**, 198, 76
[55] E.J. Crumlin, Z. Liu, H. Bluh, W. Yang, J. Guoa, Z, Hussain *Journal of Electron Spectroscopy and Related Phenomena*, **2015**, 200, 264.
[56] V. Papaefthimiou, D. K.Niakolas, F. Paloukis, D. Teschner, A. Knop-Gericke, M. Haevecker, S. Zafeiratos *J. Catal.* **2017**, 352, 305
[57] G. Nurk, T. Huthwelker, A. Braun, C. Ludwig, E.Lust, R.P.W.J. Struis *J. Power Sources* **2013**, 240, 448.
[58] K-C Chang, B. Ingram, J. Ilavsky, S. Lee, Paul Fuoss, H. You, *Solid State Ionics, **2017,*** 311, 127.
59 M. Kishimoto, M. Lomberg, E. Ruiz-Trejo, N. P. Brandon, *J. Power Sources*, **2014,** *266*, 291.
60 J. R. Ferraro, *Introductory Raman Spectroscopy*.: Academic press, London **2003.**
61 R. C. Maher, *Raman for Solid Oxide Fuel Cells*, in *Spectroscopic Properties of Inorganic and Organometallic Compounds Volume 43* (Ed. J. Yarwood) Royal Society of Chemistry: London **2012.**
62 E. Brightman, R. Maher, G. J. Offer, V. Duboviks, L. F. Cohen, N. P. Brandon, *Rev. Sci. Instrum.*, **2012**, 83, 053707.
63 R. C. Maher, P. R. Shearing, E. Brightman, D. J. L. Brett, N. P. Brandon, L. F. Cohen, *Adv. Sci.*, **2016**, 3, 1500146.
64 R. C. Maher, L. F. Cohen, P. Lohsoontorn, D. J. L. Brett, N. P. Brandon, *J. Phys. Chem. A*, **2008**, 112, 1497.
65 Z. Cheng, M. Liu, *Solid State Ionics*, **2007**. 178, 925.
66 Z. Cheng, H. Abernathy, M. Liu, *J. Phys. Chem. C*, **2007**, 111, 17997.
67 H. H. Mai Thi, B. Saubat, N. Sergent, T. Pagnier, *Solid State Ionics*, **2015**, 272**,** 84.
68 B. C. Eigenbrodt, R. A. Walker, *Anal. Methods*, **2011**, 3, 1478.
69 R. C. Maher, V. Duboviks, G. J. Offer, M. Kishimoto, N. P. Brandon, L. F. Cohen, *Fuel Cells*, **2013**, 13, 455.
70 F. Tuinstra, J. L. Koenig, *J. Chem. Phys.*, **1970**, 53, 1126.
71 A. C. Ferrari, J. Robertson, *Phys. Rev. B*, **2000**, 61, 14095.
72 M. B. Pomfret, J. Marda, G. S. Jackson, B. W. Eichhorn, A. M. Dean, R. A. Walker, *J. Phys. Chem. C*, **2008**, 112, 5232.
73 M. B. Pomfret, J. C. Owrutsky, R.A. Walker, *Anal. Chem.*, **2007**, 79, 2367.
74 M. B. Pomfret, J. C. Owrutsky, R.A. Walker, *Annu. Rev. Anal. Chem.*, **2010**, 3, 151.
75 B. C. Eigenbrodt, M. B. Pomfret, D. A. Steinhurs, J. C. Owrutsky, R. A. Walker, *J. Phys. Chem. C*, **2011**, 115, 2895.
76 M. D. McIntyre, D.M. Neuburger, R.A. Walker, *ECS Trans.*, **2015**, 66, 11.
77 J. D. Kirtley, M. B. Pomfret, D. A. Steinhurst, J. C. Owrutsky, R. A. Walker, *J. Phys. Chem. C*, **2015**, 119, 12781.
78 X. Li, M. Liu, S. Y. Lai, D. Ding, M. Gong, J. Lee, K. S. Blinn, Y. Bu, Z. Wang, L. A. Bottomley, F. M. Alamgir, M. Liu, *Chem. Mater.*, **2015**, 27, 822.
79 M. D. McIntyre, J. D. Kirtley, A. Singh, S. Islam, J. M. Hill, R. A. Walker, *J. Phys. Chem. C*, **2015**, 119, 7637.
80 T. Nagasawa, D. Chen, S. Y. Lai, M. Liu, K. Hanamura, *J. Power Sources*, **2016**, 324, 282.
81 W. Li, Y. Shi, Y. Luo, Y. Wang, N. Cai, *J. Power Sources*, **2015**, 276, 26.
82 S. Hüfner, *Photoelectron spectroscopy: principles and applications.* Springer, **1995.**
83 N. V. Skorodumova, S. I. Simak, B. I. Lundqvist, I. A. Abrikosov, B. Johansson, *Phys. Rev. Lett.*, **2002**, 89, 166601/1.
84 A. Kotani, T. Jo, J. C. Parlebas, *Adv. Phys.*, **1988**, 37, 37.
85 M. A. Henderson, C. L. Perkins, M. H. Engelhard, S. Thevuthasan, C. H. F. Peden, *Surf. Sci.*, **2003**, 526, 1.
86 A. Gupta, U. V. Waghmare, M. S. Hegde, *Chem. Mater.*, **2010**, 22, 5184.
87 A. Babaei, S.P. Jiang, J. Li, *J. Electrochem. Soc.*, **2009**, 156, 1022.
88 C. Zhang, M. E. Grass, A. H. McDaniel, S. C. DeCaluwe, F. E. Gabaly, Z. Liu, K. F. McCarty, R. L. Farrow, M. A. Linne, Z. Hussain, G. S. Jackson, H. Bluhm, B. W. Eichhorn, *Nat. Mater.*, **2010**, 9, 944.
89 Y. Yu, B. Mao, A. Geller, R. Chang, K. Gaskell, *Phys. Chem. Chem. Phys.*, **2014**, 16, 11633.
90 F. El Gabaly, K. F. McCarty, H. Bluhm, A. H. McDaniel, *Phys. Chem. Chem. Phys.*, **2013**, 15, 8334.
91 A. Nenning, A. K. Opitz, C. Rameshan, R. Rameshan, R. Blume, M. Havecker, A. Knop-Gericke, G. Rupprecher, B. Klotzer, J. Fleig, *J. Phys. Chem*., C, **2016**, 120, 1461.
92W. C. Chueh, A. H. McDaniel, M. E. Grass, Y. Hao, N. Jabeen, Z. Liu, S. M. Haile, K. F. McCarty, H. Bluhm, F. E. Gabaly, *Chem. Mater.*, **2012**, 24, 1876.
93 S.P. Jiang, *Mater. Sci. Eng., A,* **2006,** *418*, 199.

94 S.P. Jiang, *Int. J. Hydrogen Energy*, **2012,** *37*, 449.
95 R. J. Gorte, J. M. Vohs, *Curr. Opin. Colloid Interface Sci.*, **2009**, *14*, 236.
96 R. J. Gorte, S. Park, J. M. Vohs, C. Wang, *Adv. Mater.*, **2000**, *12*, 1465.
97 S. McIntosh, J. M. Vohs, R. J. Gorte, *Electrochim. Acta*, **2002**, *47*, 3815.
98 R. J. Gorte, J. M.; Vohs, *J. Catal.*, **2003**, *216*, 477.
99 S.P. Jiang, S. Zhang, Y. Zhen, W. Wang, *J. Am. Ceram. Soc.*, **2005**, *88*, 1779.
100 G. Kim, G. Corre, J. T. S. Irvine, J. M. Vohs, R. J. Gorte, *Electrochem. Solid State Lett.* **2008**, *11*, B16.
101 G. Kim, S. Lee, J. Y. Shin, G. Corre, J. T. S. Irvine, J. M. Vohs, R. J. Gorte, *Electrochem. Solid State Lett.*, **2009**, *12*, B48.
102 G. Corre, G. Kim, M. Cassidy, R. J. Gorte, J. M. Vohs, J. T. S. Irvine, *Microstructural Studies and Performance of Impregnated Manganese Containing Perovskite Solid Oxide Fuel Cell Anodes* in *Solid Oxide Fuel Cells 11* (Eds: S.C. Singhal, H. Yokokawa) Electrochemical Soc: Pennington **2009**.
103 G. Corre, G. Kim, M. Cassidy, J. M. Vohs, R. J. Gorte, J. T. S. Irvine, *Chem. Mater.*, **2009,** *21*, 1077.
104 S. Sengodan, J. Kim, J. Shin, G. Kim, *J. Electrochem. Soc.*, **2011,** *158*, B1373.
[105] Y. Li, P. Li, B. Hu, C. Xia, *J. Mater. Chem. A*, **2016**, 4, 9236.
106 G. Kaur, S. Basu, *Int. J. Energy Res.*, **2015,** *39*, 1345.
107 M. Boaro, A. Pappacena, C. Abate, M. Ferluga, J. Llorca, A. Trovarelli, *J. Power Sources*, **2014,** *270*, 79.
108 J. Kim, V. V. Nair, J. M. Vohs, R. J. Gorte, *Scripta Mater.*, **2011,** *65*, 90
109 P. Boldrin, E. Ruiz-Trejo, C. Tighe, K. C. Chang, J. Darr, N. P. Brandon, *ECS Trans.*, **2015,** *68*, 1219.
110 Z. Han, Y. Wang, Y. Yang, L. Li, Z. Yang, M. Han, *J. Alloys Compd.*, **2017,** *703*, 258.
111 C. Wu, L. Tang, M. R. De Guire, *J. Nanotechnol.*, **2014,** *5*, 1712.
112 A. Atkinson, S. Barnett, R. J. Gorte, J. T. S. Irvine, A. J. McEvoy, M. Mogensen, S. C. Singhal, J. M. Vohs, *Nat. Mater.*, **2004,** *3*, 17.
113 S. Tao, J. T. S. Irvine, *Nat. Mater.*, **2003,** *2*, 320.
114 S. Tao, J. T. S. Irvine, *J. Electrochem. Soc.*, **2004,** *151*, A252.
115 X. Zhu, Z. Lü, B. Wei, K. Chen, M. Liu, X. Huang, W. Su, *J. Power Sources*, **2009,** 190, 326.
116 X. Zhu, Z. Lü, B. Wei, Y. Zhang, X. Huang, W. Su, *Int. J. Hydrogen Energy*, **2010,** *35*, 6897.
117 Y. Li, X. Zhu, Z. Lü, Z. Wang, W. Jiang, X. Huang, W. Su, *Int. J. Hydrogen Energy*, **2014,** *39*, 7980.
118 R. Xing, Y. Wang, Y. Zhu, S. Liu, C. Jin, *J. Power Sources*, **2015,** *274*, 260.
119 X. Zhang, L. Ye, J. Hu, J. Li, W. Jiang, C.Tseng, K. Xie, *Electrochimica Acta*, **2016,** *212*, 32.
120 S. Zhu, D. Ding, M. Li, C. Xia, *J. Electrochem. Soc.*, **2017,** *164*, F916.
121 X. Yue, J. T. S. Irvine, *J. Mater. Chem. A*, **2017,** *5*, 7081.
122 C. D. Savaniu, J. T. S. Irvine, *Solid State Ionics*, **2011,** *192*, 491.
123 J. C. Ruiz-Morales, J. Canales-Vazquez, C. D. Savaniu, D. Marrero-López, W. Zhou, J. T. S. Irvine, *Nature*, **2006,** *439*, 568.
124 D. N. Miller, J. T. S. Irvine, *J. Power Sources*, **2011,** *196*, 7323.
125 M. C. Verbraeken, T. R., K. Agersted, Q. Ma, C. D. Savaniu, B. R. Sudireddy, J. T. S. Irvine, P. Holtappels, F. Tietz, *RSC Adv.*, **2015,** *5*, 1168.
126 A. D. Aljaber, J. T. S. Irvine, *J. Mater. Chem. A*, **2013**, 1, 5868.
127 M. C. Verbraeken, B. Iwanschitz, A. Mai, J. T. S. Irvine, *J. Electrochem. Soc.*, **2012,** *159*, F757.
128 M. C. Verbraeken, B. Iwanschitz, E. Stefan, M. Cassidy, U. Wissen, A. Mai, J. T. S. Irvine, *Fuel Cells*, **2015,** *15*, 682.
129 L. Lu, C. Ni, M. Cassidy, J. T. S. Irvine, *J. Mater. Chem. A*, **2016,** *4*, 11708.
130 P. K. Tiwari, X. Yue, J. T. S. Irvine, S. Basu, *J. Electrochem. Soc.*, **2017,** *164*, F1030.
131 X. Shen, K. Sasaki, *J. Power Sources*, **2016,** *320*, 180.
132 T. Ramos, S. Veltzé, B. R. Sudireddy, P. S. Jørgensen, L. T. Kuhn, P. Holtappels, *Fuel Cells*, **2014,** *14*, 1062.
133 W. Zhang, L. T. Kuhn, P. S. Jørgensen, B. R. Sudireddy, J. J. Bentzen, C. Bernuy-Lopez, S. Veltzé, T. Ramos, *J. Power Sources*, **2014,** *258*, 297.
134 J. Nielsen, T. Klemensø, P. Blennow, *J.Power Sources*, **2012,** *219*, 305.
135 E. Stefan, G. Tsekouras, J. T S Irvine, *Adv. Energy Mater.* **2013,** *3*, 1454.
136 Z. Gao, H. Wang, E. Miller, Q. Liu, D. Senn, S. Barnett, *ACS Appl. Mater. Interface*, **2017,** *9*, 7115.
[137] B. He, L. Zhao, S. Song, T. Liu, F. Chen, C. Xia, *J. Electrochem. Soc.*, **2012**, 159, B619.
[138] E. Walker, S. C. Ammal, S. Suthirakun, F. Chen, G. A. Terejanu, A. Heyden, *J. Phys. Chem. C*, **2014**, 118, 23545.
[139] Y. Wang, J. Xu, X. Meng, T. Liu, F. Chen, *Electrochem. Comm.*, **2017**, 79, 63.

[140] G. Xiao, C. Jin, Q. Liu, A. Heyden, F. Chen, *J. Power Sources*, **2012**, 201, 43.
141 H. K. Wang, Al. J. Samson, V. Thangadurai, *J. Mater. Chem. A*, **2016**, 4, 17913.
142 Z. Jiang, C. Xia, F. Chen, *Electrochimica Acta*, **2010**, 55, 3595.
143 J. M. Vohs, R. J. Gorte, *Adv. Mater.*, **2009**, 21, 943.
[144] Y. Wang, L. Zhang, C. Xia *Int. J. Hydrogen Energy*, **2012**, 37, 2182
145 R. Doshi, V. L. Richards, J. D. Carter, X. Wang, M. Krumpelt, *J. Electrochem. Soc.*, **1999**, 146, 1273.
146 S. Yoon, J. Han, S. Nam, T. Lim, I. Oh, S. Hong, Y. Yoo, H. Lim, *J. Power Sources*, **2002**, 106,160.
147 S.P. Jiang, W. Wang, J. Electrochem. Soc., **2005**, 152, A1398.
148 T. Klemensø, C. Chatzichristodoulou, J. Nielsen, F. Bozza, K. Thydén, R. Kiebach, S. Ramousse, *Solid State Ionics*, **2012**, 224, 21.
149 J. Højberg, M. Søgaard, *Electrochem. Solid-State Lett.*, **2011**, 14, B77.
150 Y. Ren, J. Ma, D. Ai, Q. Zan, X. Lin, C. Deng, *J. Mater. Chem.*, **2012**, 22, 25042.
151 Z. Liu, D. Ding, B. Liu, W. Guo, W. Wang, C. Xia, *J. Power Sources*, **2011**, 196, 8561.
152 N. Imanishi, R. Ohno, K. Murata, A. Hirano, Y. Takeda, O. Yamamoto, K. Yamahara, *Fuel Cells*, **2009**, 9, 215.
153 X. Ding, W. Zhu, G. Hua, J. Li, Z. Wu, *Electrochimica Acta*, **2015**, 163, 204.
154 B.C.H. Steele, *Solid State Ionics*, **2000**, 129, 95.
155 L. W. Tai, M. M. Nasrallah, H. U. Anderson, D. M. Sparlin, S. R. Sehlin, *Solid State Ionics*, **1995**, 76, 273.
156 T. Teraoka, H. Zhang, K. Okamoto, N. Yamazoe, *Mat. Res. Bull.*, **1988**, 23, 51.
157 H. Ding, A. V. Virkar, M. Liu, F. Liu, *Phys. Chem. Chem. Phys.*, **2013**, 15, 489.
158 E. Bucher, W. Sitte, *Solid State Ionics*, **2011**, 192, 480.
159 T. Hong, L. Zhang, F. Chen, C. Xia, *J. Power Sources*, **2012**, 218, 254.
160 B. Hu, Y. Wang, C. Xia, *J. Power Sources*, **2014**, 269, 180.
161 B. Hu, Y. Wang, C. Xia*, J. Electrochem. Soc.*, **2015**, 162, F33.
162 J. Chen, F. Liang, B. Chi, J. Pu, S.P. Jiang, J. Li, *J. Power Sources*, **2009**, 194, 275
163 L. Nie, M. Liu, Y. Zhang, M. Liu, *J Power Sources*, **2010**, 195, 4704.
164 M. Liu, D. Ding, K. Blinn, X. Li, L. Nie, M. Liu, *Int. J. Hydrogen Energy*, **2012**, 37, 8613.
165 E. Zhao, Z. Jia, L. Zhao, Y. Xiong, C. Sun, M. E. Brito, *J. Power Sources*, **2012**, 219, 133
166 J. M. Serra, H. P. Buchkremer, *J. Power Sources*, **2007**, 172, 768.
167 T. J. Huang, X. D. Shen, C. L. Chou, *J. Power Sources*, **2009**, 187, 348.
168 H. J. Hwang, J. W. Moon, S. Lee, E. A. Lee, *J. Power Sources*, **2005**, 145, 243.
169 Y. Sakito, A. Hirano, N. Inanishi, Y. Takeda, O. Yamamoto, Y. Liu, *J. Power Sources*, **2008**, 182, 476.
170 S. H. Jun, Y. R. Uhm, R. H. Song, C. K. Rhee, *Curr. Appl. Phys.*, **2011**, 11, S305.
171 T. J. Huang, C. L. Chou, *Fuel Cells*, **2010**, 10, 718.
172 S. F. Wang, C. T.; Yeh, Y. R. Wang, Y.F. Hsu, *J. Power Sources*, **2012**, 201, 18.
173 N. Lakshminarayanan, H. Choi, J. N. Kuhn, U. S. Ozkan, *Appl. Catal. B*, **2011**, 103, 318.
174 C. Gao, Y. Liu, K. Xia, S. Jiao, R.I. Tomov, R. V. Kumar, *Electrochimica Acta*, **2017**, 246, 148.
175 Y. Liu, M.; Mori, Y. Funahashi, Y. Fujishiro, A. Hirano, *Electrochem. Commun.*, **2007**, 9, 1918.
176 S. Guo, H. Wu, F. Puleo, L. F. Liotta, Catalysts 2015, 5, 366
177 M. Sahibzada, S. J. Benson, R. A. Rudkin, J. A. Kilner, *Solid State Ionics*, **1995**, 285, 113.
178 S. P. Simner, J. F. Bonnett, N. L. Canfield, K. D. Meinhardt, J. P. Shelton, V. L. Sprenkle, J. W. Stevenson, *J Power Sources*, **2003**, 1, 113.
179 V. A. C. Haanappel, D. Rutenbeck, A. Mai, S. Uhlenbruck, D. Sebold, H. Wesemeyer, B. Röwekamp, C. Tropartz, F. Tietz, *J. Power Sources*, **2004**, 130, 119.
180 C. Gao, Y. Liu, T. Zhao, W. Wand, R.I. Tomov, and R.V. Kumar, Nano-Structures & Nano-Objects, **2017 12**, 91.
181 C. Gao PhD Thesis University of Cambridge **2018**
[182] D. Ding, M. Liu, Z. Liu, X. Li, K. Blinn, X. Zhu, M. Liu *Adv. Energy Mater.*, **2013**, 3, 1149
183 T. E. Burye, J. D. Nicholas, *J. Power Sources*, **2015**, 300, 402.
184 A. Wang, L. Jia, J. Pu, B. Chi, J. Li, *Int. J. Hydrogen Energy*, **2017**, 42, 15385.
[185] Y. Gong, D. Palacio, X. Song, R. L. Patel, X. Liang, X. Zhao, J. B. Goodenough, and K. Huang, *Nano Lett.,* **2013**, 13, 4340.
186 M. Cassidy, M. Machado, P. Connor, J. Nairn, C. Ni, and J. T. S. Irvine, *11th European SOFC and SOEC Forum, A1102, 1-4 Jul 2014, Lucerne Switzerland* **2014.**
187 M. Cassidy, D. J. Doherty, X. Yue, J. T. S. Irvine, *ECS Trans.* **2015,** *68*, 2047.
188 M. C. Verbraeken, B. R. Sudireddy, V. Vasechko, M. Cassidy, T. Ramos, J. Malzbender, P. Holtappels, J. T. S. Irvine, *J. Eur. Ceram. Soc.*, **2017**, https://doi.org/10.1016/j.jeurceramsoc.2017.11.057

189 C. Ni, J. M. Vohs, R. J. Gorte, J. T. S. Irvine, *J. Mater. Chem. A*, **2014,** *2*, 19150.
[190] T. B. Hertz, T. Heiredal-Clausen, R. Küngas, *J. Electrochem. Soc.*, **2016**, 163, F38
[191] R. Kiebach, P. Zielke, J. V. T. Høgh, K. Thydén, H.-J. Wang, R. Barford, P. V. Hendriksen, *Fuel Cells* **2016**, 16, 80.